Evaluating the accuracy of methods for detecting correlated rates of molecular and morphological evolution

Yasmin Asar[1], and Hervé Sauquet[2,3], Simon Y.W. Ho[1]

[1]*School of Life and Environmental Sciences, University of Sydney, Sydney, NSW 2006, Australia*

[2]*National Herbarium of New South Wales (NSW), Royal Botanic Gardens and Domain Trust, Sydney, NSW 2000, Australia*

[3]*Evolution and Ecology Research Centre, School of Biological, Earth and Environmental Sciences, University of New South Wales, Sydney, NSW 2052, Australia*

Corresponding author: yasmin.asar@sydney.edu.au (Yasmin Asar)

Abstract.—Determining the link between genomic and phenotypic evolution is a fundamental goal in evolutionary biology. Insights into this link can be gained by using a phylogenetic approach to test for correlations between rates of molecular and morphological evolution. However, there has been persistent uncertainty about the relationship between these rates, partly because conflicting results have been obtained using various methods that have not been examined in detail. We carried out a simulation study to evaluate the performance of five statistical methods for detecting correlated rates of evolution. Our simulations explored the evolution of molecular sequences and morphological characters under a range of conditions. Of the methods tested, Bayesian relaxed-clock estimation of branch rates was able to detect correlated rates of evolution correctly in the largest number of cases. This was followed by correlations of root-to-tip distances, Bayesian model selection, independent sister-pairs contrasts, and likelihood-based model selection. As expected, the power to detect correlated rates increased with the amount of data, both in terms of tree size and number of morphological characters. Likewise, the performance of all five methods improved when there was greater rate variation among lineages. We then applied these methods to a data set from flowering plants and did not find evidence of a correlation in evolutionary rates between genomic data and morphological characters. The results of our study have practical implications for phylogenetic analyses of combined molecular and morphological data sets, and highlight the conditions under which the links between genomic and phenotypic rates of evolution can be evaluated quantitatively.

Keywords: evolutionary rates, morphological evolution, macroevolution, molecular clock, genetic drift, flowering plants

Evolution has generated the great diversity of phenotypic forms across the Tree of Life. However, the genetic mechanisms that underlie changes in phenotype remain incompletely understood (Orr 2001). It is often assumed that there is only a weak link between molecular and morphological change (Simpson 1944; Stanley 1975; Gould and Eldredge 1977; Lee et al. 2013; Halliday et al. 2019), given that the sheer number of mutations accumulating in genomes are likely to include just a small proportion that cause phenotypic changes (Gillespie 1991; Bromham et al. 2002). Furthermore, the proposal of the neutral theory of molecular evolution (Kimura 1968), which describes most mutations as having negligible impact on an organism's fitness, has bolstered the idea that molecular and morphological evolution are broadly decoupled (Bromham et al. 2002; Davies and Savolainen 2006; Lee et al. 2013; Halliday et al. 2019; Simões et al. 2020). Although genetic drift is believed to be a substantial driver of molecular evolution (Kimura 1968; Ohta 1992), morphological characters, given their importance to an organism's survival, are often assumed to be under strong selection (Lee and Palci 2015; Ho et al. 2017; Manceau et al. 2020).

Explicit tests of the link between genetic change and phenotypic change have largely focussed on model species, mapping the effect of single genes or small sets of genes (Ashton et al. 2017; Kemble et al. 2019). Recent advances in genomic sequencing have propelled studies of quantitative trait loci, where genomic regions that account for phenotypic trait variation within a species can be identified. However, these studies are time-consuming, costly, and often lack statistical power (Ashton et al. 2017). A more efficient approach that can accommodate hundreds of taxa is to assess the link between rates of molecular and morphological evolution using phylogenetic comparative methods. If there is a correlation between rates of molecular and morphological evolution, then phenotypic traits might be predominantly governed by drift rather than adaptive processes (Halliday et al. 2019), as demonstrated in the evolution of mandibles in rodents (Renaud et al. 2007) and crania in

primates (Ackermann and Cheverud 2004). Alternatively, if a species has a high rate of molecular evolution, then it might also have a high rate of morphological evolution simply because it will experience larger numbers of phenotype-altering mutations. However, apparent correlations between molecular and morphological evolutionary rates might be due to both being driven by a third factor. For example, species with small population sizes might experience rapid evolutionary change because of the heightened impacts of drift on both genomic mutations and morphological traits (Combosch et al. 2017).

To date, there have been few explicit tests of the link between molecular and morphological evolutionary rates (Seligmann 2010). Instead, indirect tests have been carried out on 'living fossils', or taxa with presumed morphological conservatism across long timescales and high evolutionary distinctiveness (Lidgard and Love 2018; Turner 2019). For instance, the tuatara (*Sphenodon punctatus*) diverged from all other squamates ~220 million years ago (Ma) and is the only extant member of the order Rhynchocephalia (Herrera-Flores et al. 2017). Despite the inference that the long lineage leading to the tuatara has experienced little morphological evolution (Herrera-Flores et al. 2017; Simões et al. 2022b), the mitochondrial control region of the tuatara has been estimated to evolve at a remarkably high rate (Hay et al. 2008; Subramanian et al. 2009). Earlier work on morphologically conserved horseshoe crabs showed only modest reductions in the rate of mitochondrial evolution compared with scorpions and brine shrimp (Avise et al. 1994). Analysis of *Ginkgo biloba*, the sole surviving species in its order, showed enrichment in duplicated genes and expansion of gene families, bolstering complex chemical defence mechanisms against herbivory (Guan et al. 2016; Šmarda et al. 2016). These results suggest a decoupling of the rates of molecular and morphological evolution in some taxa. In contrast, however, recent transcriptomic analyses of 'living fossils' have shown reduced rates of molecular evolution across hundreds of protein-coding genes in *Nautilus* (Combosch et al. 2017; Zhang et al. 2021; Huang et al.

2022; Sanchez et al. 2022), the African coelacanth (Amemiya et al. 2013), the tuatara (Gemmell et al. 2020), and in long-lived sacred lotus (Ming et al. 2013).

Phylogenetic studies of the relationship between morphological and molecular evolutionary rates have produced a mixture of results. An analysis of 13 vertebrate data sets yielded no evidence for an association between rates of molecular and morphological evolution (Bromham et al. 2002), contradicting the results of an earlier study that detected such a correlation in seven of the eight diverse data sets analysed (Omland 1997). Although most studies have tested evolutionary rate correlations in animals, analyses of small data sets from angiosperms (flowering plants) have found weak but positive correlations between rates of molecular and phenotypic evolution (Omland 1997; Barraclough and Savolainen 2001; Davies and Savolainen 2006). These positive correlations have been found across many angiosperm taxa, including: *Sedum* (family Crassulaceae), *Krigia* (family Asteraceae), birch (family Betuleacae), spindle trees (family Celastraceae), Hypoxidaceae, walnuts (family Juglandaceae), *Protea* (family Proteaceae), buckthorns (family Rhamnaceae), and monocots. By gaining insights into the relationship between molecular and morphological evolution in such an extraordinarily species-rich and hyperdiverse group (Onstein 2019), we can achieve a better understanding of the rapid ecological dominance of angiosperms and their evolutionary dynamics (Sauquet and Magallon 2018).

The persistent uncertainty about the relationship between molecular and morphological rates is compounded by the lack of a detailed investigation of the conditions under which a correlation can be detected (Simpson 1944; Seligmann 2010). Without the use of post hoc power analyses (e.g., Davies and Savolainen 2006), it is unclear whether insufficient statistical power in analyses precludes detection of correlated rates or if there is a genuine lack of an association. This is especially pertinent given that previous broad-scale studies examined small sets of genetic markers, commonly ‘housekeeping’ genes (Omland

1997; Barraclough and Savolainen 2001; Davies and Savolainen 2006). These genes might not be well-suited for comparison with morphological rates, since they are under functional constraints and are unlikely to be representative of genome-wide patterns (Bromham et al. 2002). In addition, there remain questions about methodology, such as whether terminal branches of trees inferred with morphological data should be included when testing for correlations between rates of morphological and molecular evolution, given that they might underestimate the amount of evolutionary change (Bromham et al. 2002; Seligmann 2010). This is because autapomorphies (changes that have occurred only in single taxa) are often excluded when collecting morphological characters (Wright and Hillis 2014). Furthermore, previously applied approaches such as root-to-tip distance correlations have been criticized for their time-averaging effect and for the inclusion of non-independent data points, thereby increasing the risk of spurious positive correlations (Felsenstein 1985; Bromham et al. 2002; Rambaut et al. 2016; Barba-Montoya et al. 2021). Thus, it remains unclear whether the mixed results from previous studies have been due to the use of different data sets, insufficient statistical power, or the use of varied methods to test for rate correlations.

Here we aim to uncover the conditions under which correlations between molecular and morphological rates of evolution can be detected. We present a comprehensive simulation study based on parameters from angiosperms, which lends reality to our estimates. We evaluate five approaches for detecting correlated rates of evolution under these conditions, including root-to-tip distance correlations, independent sister-pairs contrasts, likelihood-based model selection, correlations of Bayesian branch rates inferred using relaxed clocks, and Bayesian model selection. Using the insights provided by the simulation study, we test for evolutionary rate correlations between angiosperm floral characters and genomic DNA. Our analyses have implications for understanding the relationship between genotypic

and phenotypic change and inform practical recommendations for detecting correlated evolutionary rates.

MATERIALS AND METHODS

Simulations of Molecular and Morphological Evolution

Phylogenetic trees and evolutionary rates.—We performed simulations using chronograms (branch lengths measured in millions of years, Myr) of three different sizes, based on a 792-species angiosperm tree from Magallón et al. (2015) used by Sauquet et al. (2017). From this tree, we sampled 18, 45, or 111 species to represent diverse angiosperm lineages (Fig. 1a). These three trees had root ages of 139.40 Ma.

We rescaled the branch lengths of the chronograms to produce phylograms (where branch lengths measured in substitutions/site). To do this, we used the R package *NELSI* (Ho et al. 2015) to generate branch lengths according to an uncorrelated lognormal clock (Drummond et al. 2006). The branch rates had a mean of 9.65×10^{-4} subs/site/Myr, inferred in a previous analysis of two nuclear markers (18S and 26S ribosomal DNA) and three plastid protein-coding genes (*atpB*, *rbcL*, and *matK*) from 792 angiosperm species (Magallón et al. 2015). We generated branch rates with low, moderate, and high levels of variation, with respective standard deviations of 0.25, 0.75, and 1.25.

We then performed simulations under two scenarios, in which molecular and morphological evolutionary rates were either correlated or uncorrelated. To generate a morphological phylogram with branch rates correlated with those of the molecular phylogram, we scaled the branch lengths of the latter by a factor of 1.90 (Fig. 1a). This scaling factor was based on a mean rate of morphological evolution of 1.83×10^{-3} changes/character/Myr, inferred from 27 floral characters for 792 angiosperm species (Sauquet et al. 2017).

For our simulations with branch rates being uncoupled between molecular and morphological data sets, we simply used *NELSI* to generate independent sets of branch rates and used these to rescale the branch lengths of the chronograms (Fig. 1a). Mean evolutionary rates and standard deviations were as described above for the simulations with correlated branch rates between molecular and morphological data sets.

Generating molecular sequence alignments and morphological character matrices.—We used Seq-Gen version 1.3.4 (Rambaut and Grass 1997) to simulate the evolution of nucleotide sequences on the phylograms produced by the previous step (Fig. 1a). These simulations produced sequence alignments with lengths of 1000 nucleotides, reflecting typical sizes of nuclear and plastid protein-coding genes. The nucleotide transition rates, frequencies, and gamma shape parameters (degree of among-site rate variation) were based on estimates from Magallón et al. (2015) and are listed in the Supplementary Material.

We generated morphological data matrices consisting of 10, 100, and 1000 characters (Fig. 1a). Matrices with either two-state (binary) or four-state characters were simulated. Character evolution was simulated using the R package *geiger* (Pennell et al. 2014) under the Mk model (Lewis 2001), a generalization of the Jukes-Cantor (1969) model of molecular evolution. The relative rate for each character was drawn randomly from a gamma distribution with a shape parameter of 1.39 inferred via maximum-likelihood analysis of the floral character data set from Schönenberger et al. (2020), comprising 30 binary and multi-state morphological characters scored for 792 angiosperm species (see Supplementary Material). This morphological data set was also used in the empirical analyses in this study.

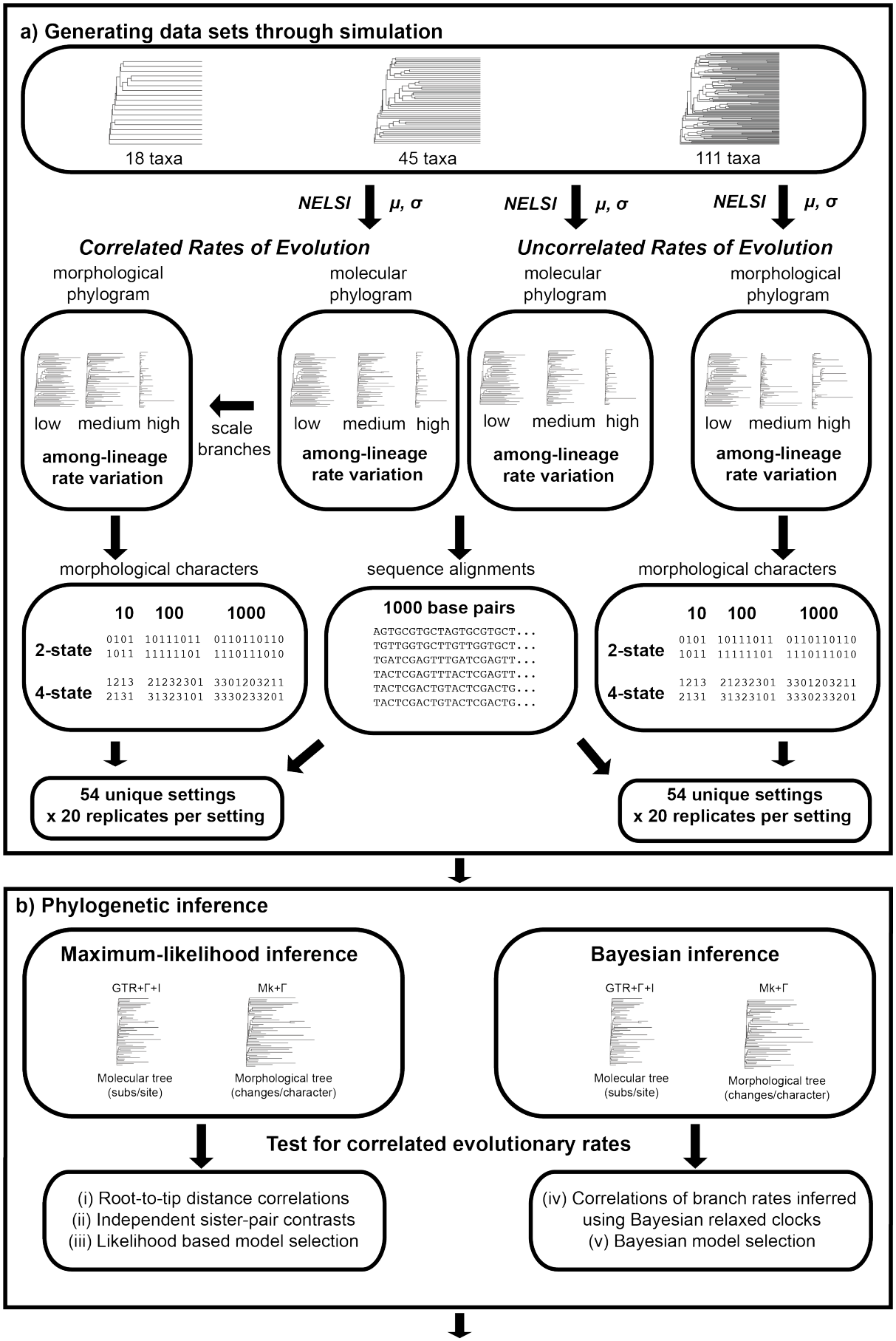

183

FIGURE 1. Flowchart of simulation study. a) Generating data sets through simulation. Molecular phylograms are generated using chronograms with three tree sizes (18, 45, or 111 taxa), with a mean rate of evolution (μ) that has been inferred from an empirical data set, and standard deviation (σ) representing three levels of among-lineage rate variation (0.25, 0.75 or 1.25). The branch lengths of the molecular phylogram are then multiplied by an empirical scaling factor to obtain a morphological phylogram with correlated rates of evolution along each branch. To obtain trees without correlated rates of evolution, morphological phylograms are simply generated using an independent mean rate of evolution (μ), but on the same chronogram and with the same standard deviation (σ) as the molecular phylogram. Simulations were performed under a total of 54 distinct settings each for the scenario with correlated and uncorrelated rates of evolution, with 20 replicates per setting. b) Phylogenetic inference. Using a fixed tree topology, molecular and morphological branch lengths were inferred using maximum-likelihood and Bayesian analyses. Marginal likelihoods were estimated for the purpose of Bayesian model selection. Five methods were used to test for correlated rates of evolutionary change, (*i*) root-to-tip distance correlations, (*ii*) independent sister-pairs contrasts, (*iii*) likelihood-based model selection, (*iv*) correlations of Bayesian branch rates, and (*v*) Bayesian model selection. c) Evaluate performance of methods. We compared the accuracy and power of the five methods of testing for correlated rates of evolutionary change.

Summary of simulation scenarios.—The settings described above yielded a total of 54 distinct simulation scenarios. Our simulations included trees of three sizes (18, 45, and 111 taxa). Nucleotide sequences consistently had a length of 1000 nucleotides, but we varied the number of morphological characters (10, 100, and 1000 characters) and the number of possible morphological character states (either two- or four-state characters). We simulated three levels of among-lineage rate heterogeneity with standard deviations of 0.25, 0.75, and 1.25 for the molecular and morphological data sets (Fig. 1a). For each of the 54 simulation settings, we generated 20 replicate data sets. Thus, our simulations produced a total of 1080 pairs of molecular and morphological data sets for each of the 'correlated' and 'uncorrelated' settings.

Phylogenetic Inference

Maximum-likelihood inference.—We inferred phylograms from the simulated molecular and morphological data sets using maximum likelihood in IQ-TREE2 (version

2.0.6; Bui et al. 2020) (Fig. 1b). In each analysis, the tree topology was constrained to match that used for simulation, with the addition of one outgroup taxon, the gymnosperm *Welwitschia mirabilis*. Analyses of the molecular data used the general-time-reversible model, with gamma rate heterogeneity (four discrete categories) and invariant sites (GTR+Γ+I). Analyses of the morphological data used the time-homogeneous Mk model, with empirical state frequencies and gamma rate heterogeneity with four discrete categories (Mk+Γ) (Supplementary Material). Following maximum-likelihood inference, the gymnosperm outgroup was removed from each tree. The branch lengths from these phylograms were used for root-to-tip distance correlations, independent sister-pairs contrasts, and likelihood-based model selection, which are described in the next section.

Bayesian inference.—We analysed the molecular and morphological data using Bayesian inference in BEAST2 version 2.6.2 (Bouckaert et al. 2019) (Fig. 1b). In each analysis, the tree topology was constrained to match that used for simulation. Molecular and morphological data were partitioned so that they were assigned distinct substitution models, with the GTR+Γ+I model for the molecular data set and the Mk+ Γ model for the morphological data set. The molecular and morphological data sets were assigned separate uncorrelated lognormal relaxed clocks, with the mean rate of each of these having a uniform prior between 0 and 1. The molecular and morphological data subsets shared the same fixed tree topology, with a birth-death tree prior. We also performed an analysis in which molecular and morphological data shared the same uncorrelated lognormal relaxed clock, to allow comparison between linked and unlinked clock models using Bayesian model selection.

For each Bayesian analysis, the posterior distribution was estimated using Markov chain Monte Carlo (MCMC) sampling. We ran two independent chains, each of 10,000,000 steps, with samples drawn every 1000 steps. The first 10% of samples were discarded as

244 burn-in. After checking for convergence and sufficient sampling (effective sample sizes of
245 parameters greater than 200) using the LogAnalyzer function in BEAST, we combined the
246 samples from the two chains. The tree samples were summarized using TreeAnnotator, part
247 of the BEAST package. We obtained the estimates of branch rates from the summarized trees
248 and used them in our tests of rate correlations, described below.
249
250 *Testing for Correlated Rates of Evolution*
251 We evaluated the performance of five methods for testing for correlated evolutionary
252 rates: (*i*) root-to-tip distance correlations, (*ii*) independent sister-pairs contrasts, (*iii*)
253 likelihood-based model selection, (*iv*) correlations of Bayesian branch rates, and (*v*) Bayesian
254 model selection (Fig. 1b). The first three methods were performed on maximum-likelihood
255 trees that were inferred from the simulated data. The last two methods were performed using
256 the results of our Bayesian phylogenetic analyses.
257
258 *(i) Root-to-tip distance correlations*.—The first method of testing for correlated rates
259 was based on examination of the root-to-tip distances in the maximum-likelihood
260 phylograms. Since all of the tips represent present-day taxa and are separated from the root
261 node by the same amount of time, any differences in the root-to-tip distances reflect
262 differences in evolutionary rates (Omland 1997; Bromham et al. 2002; Arab et al. 2020). For
263 each matched pair of molecular and morphological phylograms, we calculated patristic root-
264 to-tip distances using the distRoot function in the R package *adephylo* (Jombart et al. 2010)
265 and tested for a correlation between the molecular and morphological root-to-tip distances.
266 To address non-independence among the root-to-tip distances, we calculated the *p*-value
267 using a permutation test in the R package *jmuOutlier* (Higgins 2004; Garren 2019), with
268 20,000 replicates.

269

270 *(ii) Independent sister-pairs contrasts*.—The second method of testing for correlated
271 rates involved taking phylogenetically independent pairs of taxa (sister pairs) and comparing
272 their relative branch lengths between the molecular and morphological phylograms. We
273 selected sister species that shared a most recent common ancestor to the exclusion of other
274 sister pairs, which avoids the problem of phylogenetic non-independence but reduces the
275 amount of data (Felsenstein 1985; Bromham et al. 2002). We used the R package *diverge* to
276 extract sister pairs for each tree (Anderson and Weir 2022). Lists of sister pairs for each tree
277 size are provided in the Supplementary Material. By definition, the two branches in each
278 sister pair have been evolving for the same amount of time, such that their phylogram length
279 reflects their relative evolutionary rate. We computed the difference between the branch
280 lengths of sister species in the molecular and morphological phylograms inferred using
281 maximum likelihood. We tested for correlations between the molecular and morphological
282 contrasts using the non-parametric Spearman's rank correlation test, to allow for violations of
283 bivariate normality and homoscedasticity. The contrasts were log-transformed and
284 standardized following standard guidelines by dividing by the square root of the time since
285 divergence between sister species (see Supplementary Materials for details; Garland et al.
286 1992; Freckleton 2000; Welch and Waxman 2008).

287

288 *(iii) Likelihood-based model selection*.—The third method of testing for correlated
289 rates involved likelihood-based model selection using information criteria. We analysed the
290 molecular and morphological data using maximum likelihood in IQ-TREE2 and compared
291 models in which the branch lengths were either linked ('proportionate') or unlinked between
292 the molecular and morphological trees. These two models reflect correlated and uncorrelated
293 branch rates, respectively, between molecular and morphological data (Duchêne et al. 2020).

We compared the models using the corrected Akaike information criterion (AICc) and the Bayesian information criterion (BIC).

(iv) Correlations of Bayesian branch rates.—The fourth method of testing for correlated rates was based on the inferred branch rates from Bayesian phylogenetic analyses. We tested for correlations between the branch rates inferred using the uncorrelated lognormal relaxed clock for the molecular and morphological data sets. To compute the significance of the correlation, we used Spearman's rank-order correlation test to avoid violations of bivariate normality and homoscedasticity. For comparison, tests were performed using the mean and median posterior branch rates. The mean posterior rate is commonly reported in Bayesian phylogenetic analyses, but the median rate might be more appropriate because the marginal posterior distributions are skewed.

(v) Bayesian model selection.—The fifth method of testing for correlated rates involved the use of Bayesian model selection to compare the support for linked or unlinked branch rates between molecular and morphological data. Model selection was performed using Bayes factors, which compare the marginal likelihoods of the two models. The marginal likelihoods of the linked and unlinked relaxed-clock models were estimated using the 'MS' Model Selection package in BEAST2. We used generalized-stepping-stone sampling (Baele et al. 2016), with 25 steps and chain lengths of 400,000. The ratio of the marginal likelihoods was used to compute the Bayes factor, which was then interpreted using the guidelines of Kass and Raftery (1995).

Evaluation of performance.—We used two approaches to evaluate the performance of the five methods of testing for rate correlations. First, we evaluated the methods by their

power, which is the ability to detect positive correlations under the largest number of scenarios. Second, we examined the accuracy of the methods, regarded here as the ability to detect positive correlations without false positives. We do not attempt to evaluate the ability of the methods to infer the correct *degree* of rate correlation, i.e., the correlation coefficient.

Case Study: Flowering Plants

To test for correlated rates of molecular and morphological evolution in empirical data, we applied the above five methods to large angiosperm data sets. Molecular data were obtained from the One Thousand Plant Transcriptomes Initiative (2019), hereafter ONEKP. This data set includes nucleotide sequences from 410 protein-coding nuclear genes from 1,124 green plants, glaucophytes, and red algae. For computational tractability, we analysed a subset of 111 angiosperm species and one gymnosperm outgroup (*Welwitschia mirabilis*), matching the angiosperm species in the morphological data set. We applied the data-partitioning scheme as outlined by ONEKP (2019) and estimated branch lengths on a fixed tree topology using maximum-likelihood analysis and Bayesian inference. The substitution model for each data subset was selected using ModelFinder in IQTREE2 (Kalyaanamoorthy et al. 2017).

The morphological data set was sourced from Schönenberger et al. (2020), representing a slightly expanded data set of 30 floral characters for 792 angiosperm species, initially published by (2017). These are discrete binary and multi-state morphological characters, including features such as the structural sex of flowers, ovary position, phyllotaxy, number of reproductive parts, and fusion of ovaries. We used a subset of 111 angiosperm species for our analyses and partitioned the data according to the number of character states (i.e., two-, three-, four-, and five-state data were treated as separate subsets). Branch lengths were estimated on a fixed tree topology using maximum-likelihood analysis and Bayesian

inference, using the Mk+Γ model of evolution with correction for ascertainment bias. The model was selected using ModelFinder in IQ-TREE2.

We performed Bayesian phylogenetic analyses of the genomic data and floral characters with and without calibrations. In the former case, we implemented secondary calibrations on the ages of key angiosperm groups. The secondary calibrations were sourced from Ramírez-Barahona et al. (2020) and applied as normal priors on node ages (Ho and Phillips 2009). To estimate the posterior distribution, we sampled from five independent MCMC runs with chain lengths of either 50 or 70 million steps. Samples were drawn every 1000 steps. After checking for convergence and sufficient sampling in Tracer, we removed a burn-in fraction of between 40% and 60%, depending on the analysis, leaving a total of 170,000 sampled trees. Further details of the angiosperm case study, including settings and secondary calibrations, are available in the Supplementary Material.

We tested for correlations between rates of nuclear genomic evolution and floral character evolution using (*i*) root-to-tip distance correlations, (*ii*) independent sister-pairs contrasts, (*iii*) likelihood-based model selection, (*iv*) correlations of Bayesian branch rates, and (*v*) Bayesian model selection. We checked assumptions for each of these tests, as described in the Supplementary Material.

RESULTS

Performance in Detecting Correlated Evolutionary Rates

Using data generated by simulation, we compared five methods for testing for correlations in evolutionary rates between molecular sequences and morphological characters. Correlations of branch rates from Bayesian relaxed-clock inference were able to detect correlated rates between molecular and morphological data under the widest range of simulation settings (Fig. 2 and 3). Under this method, the mean and median posterior branch

rates were equally effective, with an average detection of correlated evolutionary rates of 85.8% and 85.6%, respectively. The performance of this method was closely followed by root-to-tip distance correlations (84.9%), Bayesian model selection (64.4%), and independent sister-pairs contrasts (48.2%) (Fig. 2; and 3). Likelihood-based model selection had very high detection of correlated evolutionary rates across scenarios (97.0% with AICc and 100% with BIC) but had an unacceptably high frequency of false positives.

When we analysed molecular and morphological data sets that had been generated without correlated rates, we found low false-positive rates when using correlations of Bayesian branch rates (1.20% and 2.96% for mean and median posterior branch rates, respectively), root-to-tip distance correlations (7.96%), independent sister-pairs contrasts (3.06%), and Bayesian model selection (3.06%) (Fig. 3 and 4). However, likelihood-based model selection yielded a high frequency of false positives when using either the AICc (47.3%) or BIC (69.3%).

Impacts of Varying Simulation Conditions

We tested the effect of tree size, including 18, 45, and 111 taxa in the simulations, to evaluate its impact on the ability to detect correlated evolutionary rates. The number of taxa influenced the detection of correlations predictably (Fig. 5a), with performance increasing with tree size (57.7%, 81.1%, and 82.5% for tree sizes of 18, 45, and 111 taxa, respectively). Analyses of the 18 taxon-set performed poorly when there were only 10 morphological characters (Fig. 2). This was especially apparent for independent sister-pairs contrasts, where analyses of 18-taxon data sets failed to detect rate correlations regardless of the degree of among-lineage rate variation, number of character states, and numbers of morphological characters.

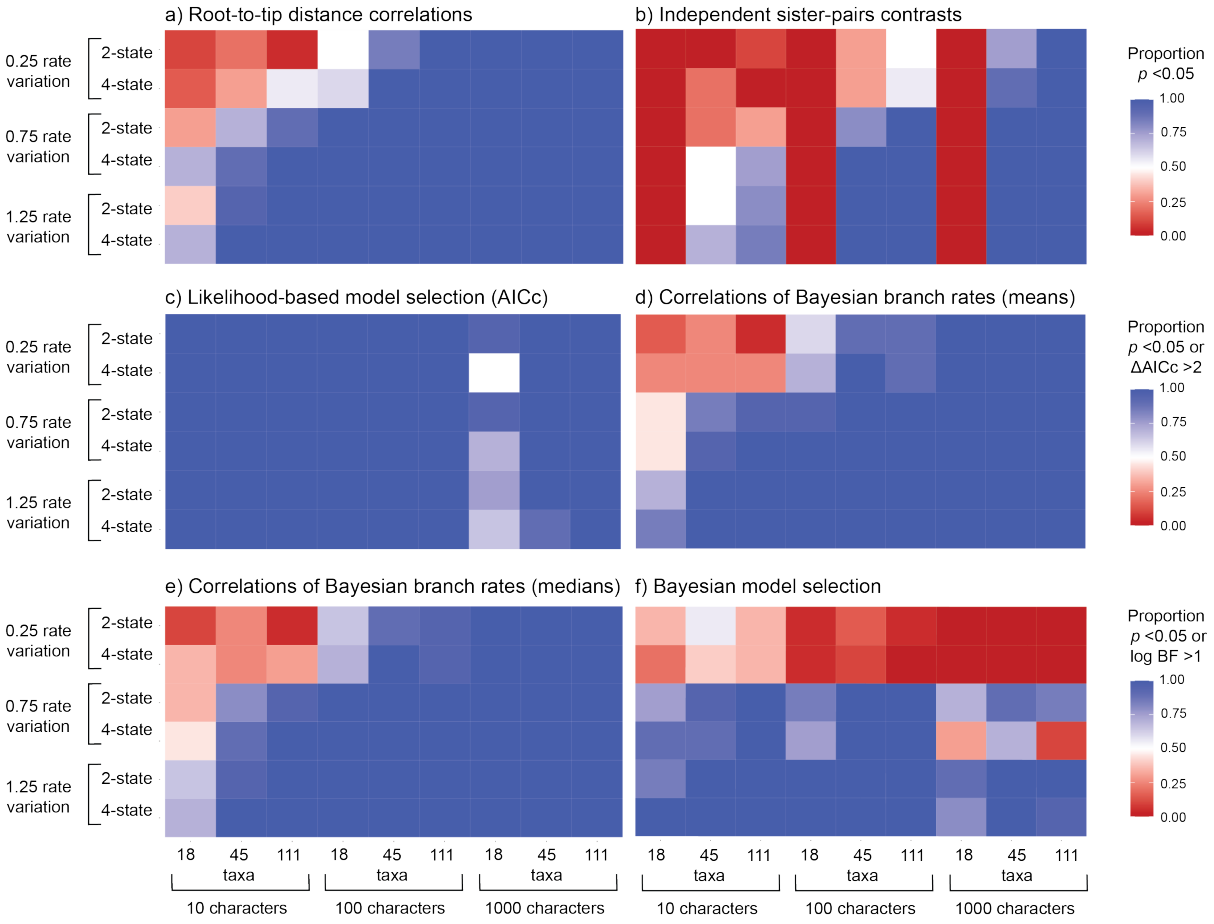

FIGURE 2. Heatmaps showing the performance of five approaches for testing for correlations between molecular and morphological evolutionary rates, for data produced by simulation with correlated evolutionary rates: a) root-to-tip distance correlations; b) independent sister-pairs contrasts; c) likelihood-based model selection using the corrected Akaike information criterion (AICc); correlations of Bayesian branch rates using d) mean posterior branch rates of branches or e) median posterior branch rates; and f) Bayesian model selection. In each panel, rows give results under six scenarios, representing combinations of three levels of among-lineage rate variation [0.25, 0.75, 1.25], and either two- or four-state morphological characters. In each panel, columns give results for data sets of various sizes, representing combinations of three numbers of morphological characters [10, 100, 1000] and three numbers of taxa [18, 45, 111]. For methods (a)–(b) and (d)–(e), colours indicate the proportion of 20 replicates for each setting that yielded a significant rate correlation (i.e., $p < 0.05$). For method (c), colours indicate the proportion of 20 replicates for each setting that yielded ΔAICc > 2, supporting a model of linked rates over a model of unlinked rates. For method (f), colours indicate the proportion of 20 replicates for each setting that yielded a log Bayes factor (BF) > 1.0 for a model of linked rates over a model of unlinked rates. For heatmaps of likelihood-based model selection using the Bayesian information criterion, see Supplementary Material.

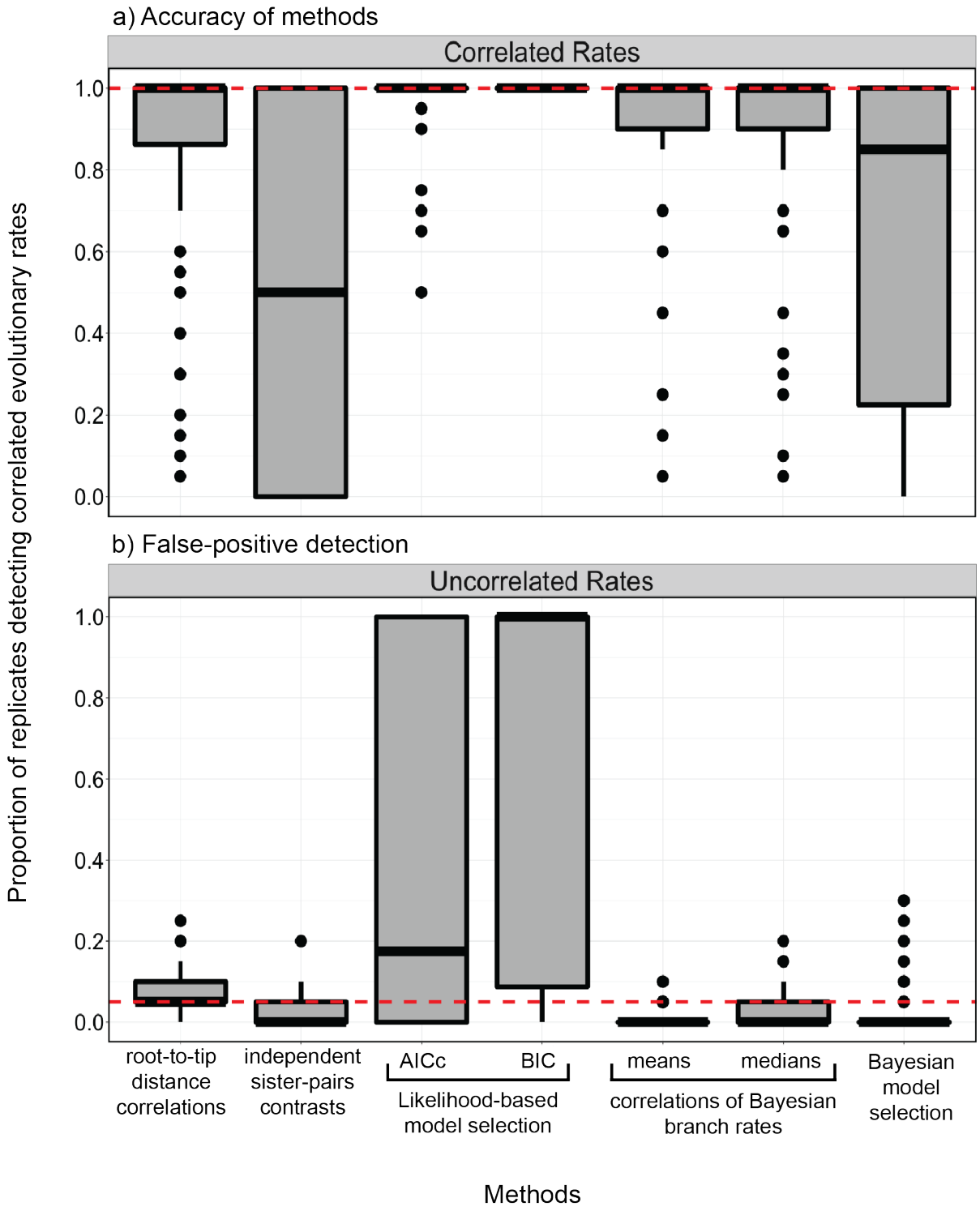

Figure 3. Boxplots showing the frequency of detecting correlated rates of evolution between simulated molecular and morphological data using different methods. A) Accuracy of the methods when analysing data simulated with correlated rates. The dashed horizontal line represents the ideal detection of correlated rates of evolution (100% of scenarios). B) Propensity of methods to detect correlations when analysing data simulated with uncorrelated rates (false positive detection). The dashed horizontal line represents the detection of correlated rates of evolution expected under frequentist statistics with a critical value of 0.05 (false positive rate of 5%).

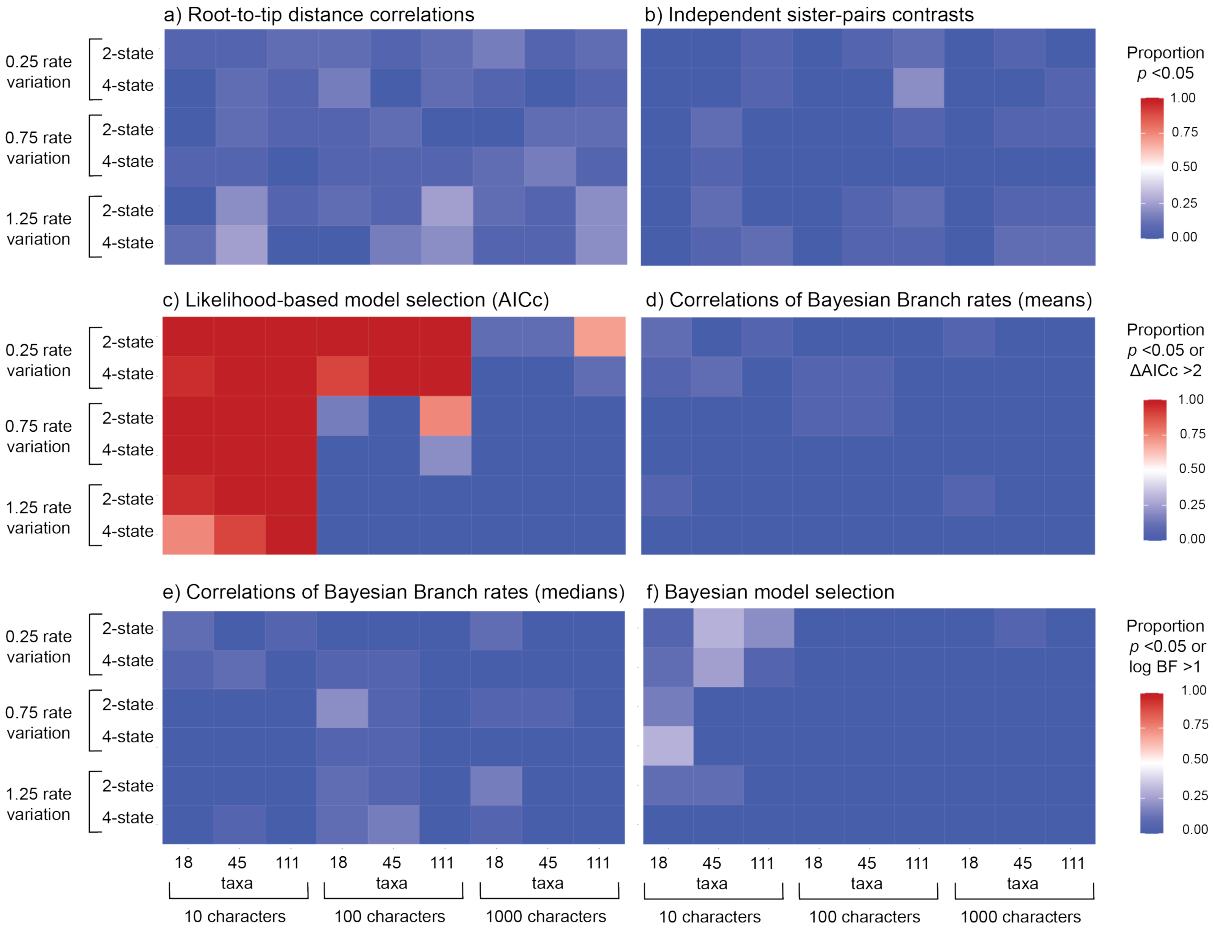

FIGURE 4. Heatmaps showing the performance of five approaches for testing for correlations between molecular and morphological evolutionary rates, for data produced by simulation without correlated evolutionary rates: a) root-to-tip distance correlations; b) independent sister-pairs contrasts; c) likelihood-based model selection using the corrected Akaike information criterion; correlations of Bayesian branch rates using d) mean posterior branch rates of branches or e) median posterior branch rates; and f) Bayesian model selection. In each panel, rows give results under six scenarios, representing combinations of three levels of among-lineage rate variation [0.25, 0.75, 1.25], and either two- or four-state morphological characters. In each panel, columns give results for data sets of various sizes, representing combinations of three numbers of morphological characters [10, 100, 1000] and three numbers of taxa [18, 45, 111]. For methods (a)–(b) and (d)–(e), colours indicate the proportion of 20 replicates for each setting that yielded a significant rate correlation (i.e., $p < 0.05$). For method (c), colours indicate the proportion of 20 replicates for each setting that yielded ΔAICc > 2, supporting a model of linked rates over a model of unlinked rates. For method (f), colours indicate the proportion of 20 replicates for each setting that yielded a log Bayes factor (BF) > 1.0 for a model of linked rates over a model of unlinked rates. For heatmaps of likelihood-based model selection using the Bayesian information criterion, see Supplementary Material.

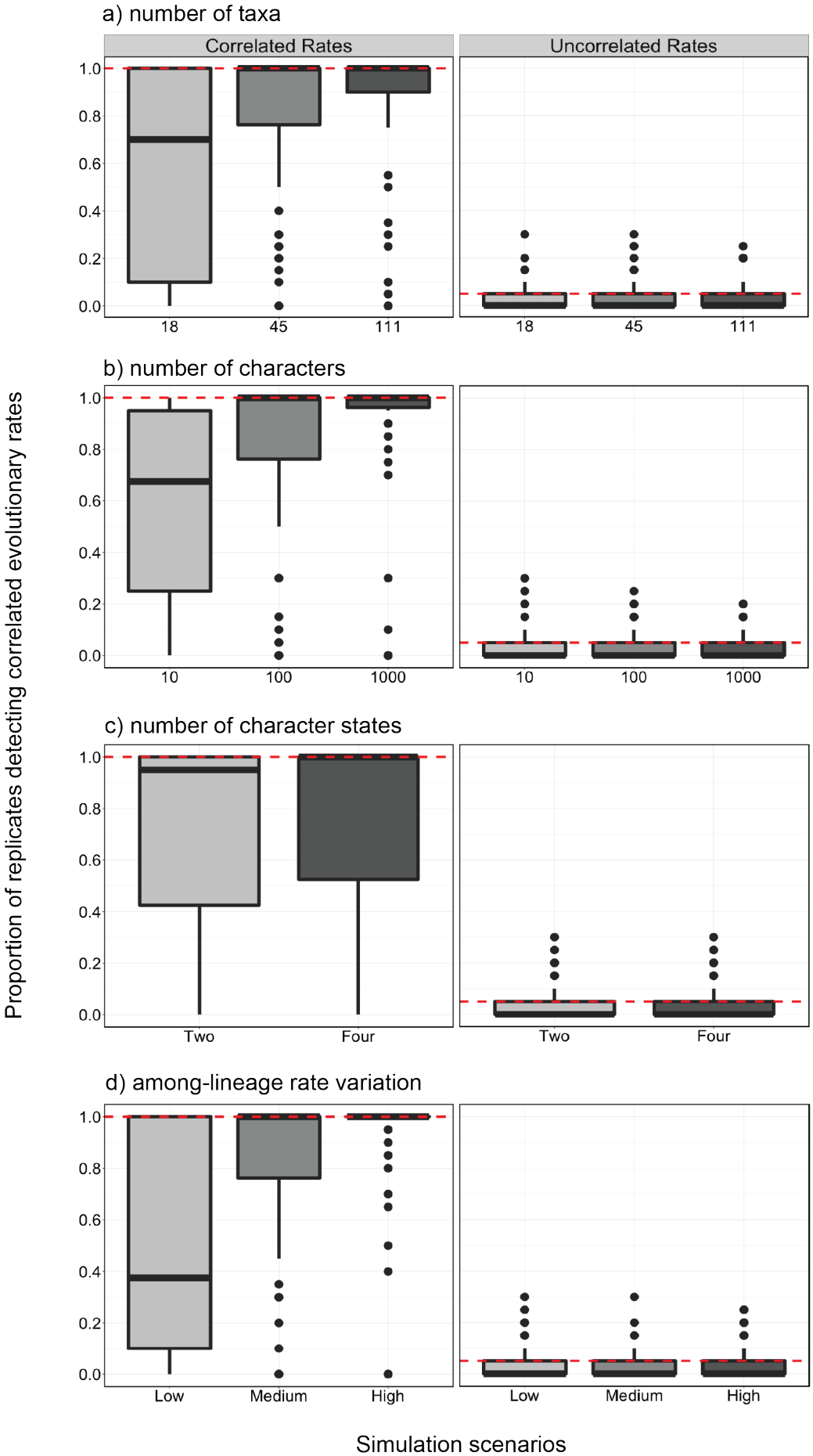

FIGURE 5. Boxplots showing the frequency of detecting correlated rates of evolution between simulated molecular and morphological data using different settings. The left panels show the performance of methods when data were simulated with correlated rates, with dashed horizontal lines representing the ideal detection of correlated rates of evolution (100% of scenarios). The right panels show results when simulated with uncorrelated rates, with dashed horizontal lines representing the detection of correlated rates of evolution expected under frequentist statistics with a critical value of 0.05 (false positive rate of 5%). The different settings used were: a) three tree sizes, b) three sizes of morphological character matrices, c) two numbers of possible morphological character states, and d) three levels of among-lineage rate variation. The results were pooled across all methods except for likelihood-based model selection, since this method had such a high rate of false positives and would unreasonably skew the detection of correlations. Boxplots calculated with the results from likelihood-based model selection can be found in the Supplementary Material.

We varied the number of morphological characters [10, 100, 1000] to evaluate their impact on the ability of the five methods to detect correlated evolutionary rates. We found that the average detection of positive correlations increased from 57.6%, 80.6%, to 83.2% for data sets with 10, 100, and 1000 morphological characters, respectively (Fig. 2 and 5b). We found that the effect depended on the amount of among-lineage rate variation; where branch rates had a standard deviation of at least 0.75, the four best approaches were generally able to detect correlations with any number of morphological characters (Fig. 2). However, when there was a low degree of among-lineage rate variation, rate correlation could not be detected when there were only 10 morphological characters. Furthermore, likelihood-based model selection detected a high rate of false positives, but this was mitigated when there were either 100 or 1000 morphological characters and moderate or high among-lineage rate variation (Fig. 4c and Supplementary Material).

The number of character states for the morphological data had a minor impact on detection of correlations. Generally, correlations were more frequently detected when the morphological data comprised four-state characters, with a positive detection of 75.1% compared with 72.4% when the data comprised two-state characters (Fig. 2 and 5c), although this effect was negligible when there were greater than 10 morphological characters and 18 taxa in the data set (Fig. 3).

476 Across the four most powerful and accurate methods, the most important factor for
477 detection of correlated evolutionary rates was among-lineage rate variation (Fig. 2 and 5d).
478 When we implemented low among-lineage rate variation in the data sets, correlated rates
479 could only be detected across 50.2% of replicates, whereas medium and high levels increased
480 detection to 81.9% and 89.2%, respectively. Where there was low among-lineage rate
481 variation, with branch rates having a standard deviation of 0.25, the four best approaches
482 were generally unable to detect correlations without sampling at least 100 morphological
483 characters (Fig. 2). This was especially true for Bayesian model selection, which could not
484 detect correlated rates of evolution at the lowest level of among-lineage rate variation.
485
486 *Case Study: Flowering Plants*
487 In our analyses of genomic DNA and floral characters in angiosperms, we found that
488 two of the five methods, root-to-tip distance correlations and likelihood-based model
489 selection, detected a correlation in evolutionary rates. We found evidence of a correlation in
490 our analysis of root-to-tip distances ($p \approx 0$; Fig. 6a). Outliers (data points outside 1.5 times
491 the interquartile range) were excluded from the permutation test, but root-to-tip distances
492 were significantly correlated both before and after removal of outliers (see Supplementary
493 Material). These outliers included the branch leading to the sister taxon to all remaining
494 angiosperms, *Amborella trichopoda*, which had a low morphological evolutionary rate of
495 2.38×10^{-6} changes/character/Myr. Other ANA-grade angiosperms, such as *Austrobaileya*
496 *scandens* and *Illicium floridanum*, similarly had low rates of morphological change and were
497 removed from the test. Likelihood-based model selection also yielded strong support for
498 linking branch lengths between nuclear sequences and floral characters, when using both
499 AICc (ΔAICc = 203.4) and BIC scores (ΔBIC = 2504.9).

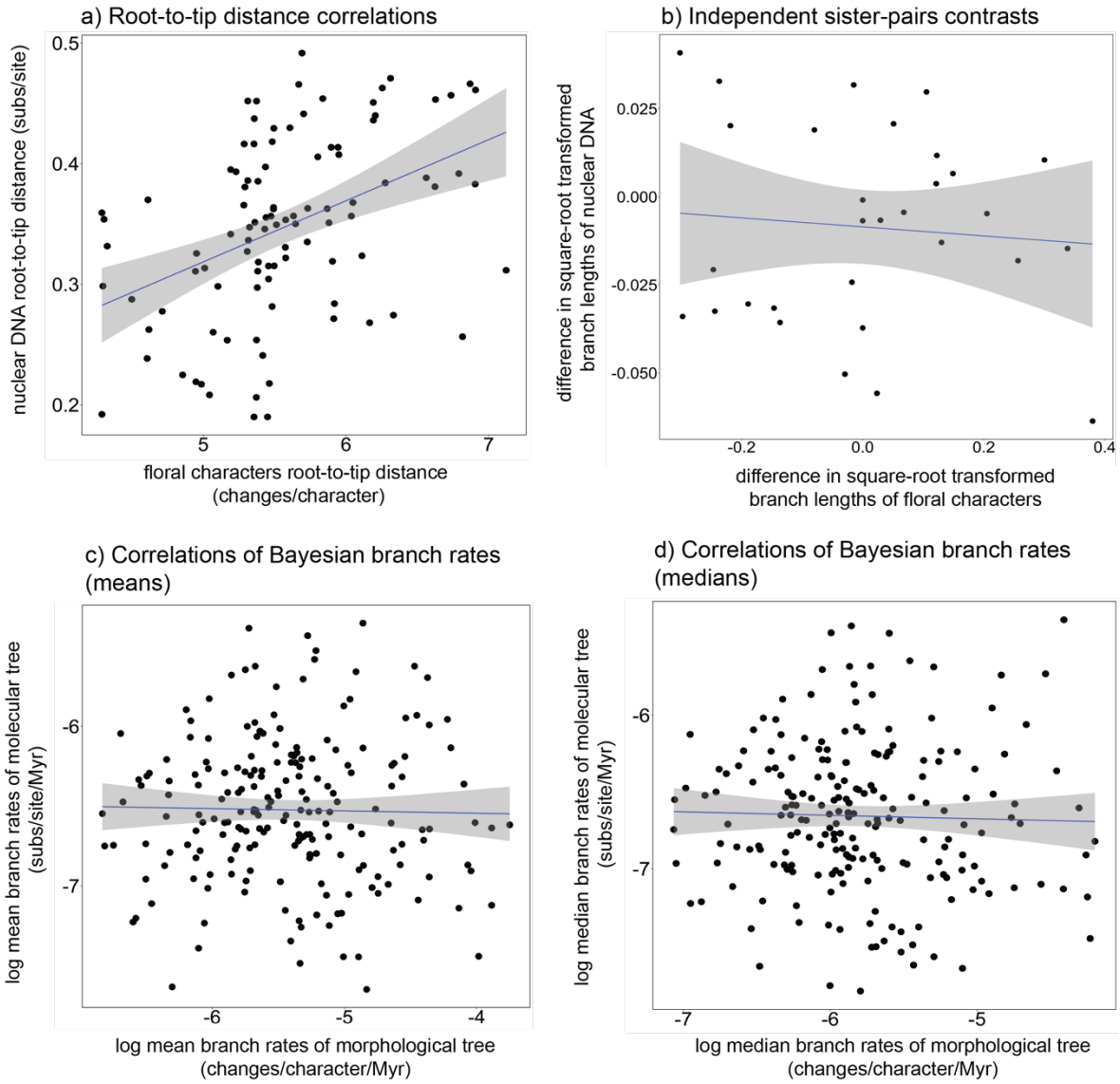

Figure 6. Comparisons between evolutionary rates of nuclear genomic DNA and floral characters inferred from angiosperms. The methods used to test for correlated rates of evolution are a) root-to-tip distance correlation; b) independent-sister pairs contrasts; c) correlations of Bayesian mean posterior branch rates; and d) correlations of Bayesian median posterior branch rates. The plot for each comparison has been fit with a linear model, which is displayed along with the 95% confidence interval.

We found no evidence of correlated molecular and morphological rates when we analysed the data using independent sister-pairs contrasts (r_s = 0.0162, p = 0.466; Fig. 6b), correlations of Bayesian mean posterior branch rates (r = –0.0209, p = 0.617; Fig. 6c), or correlations of Bayesian median posterior branch rates (r_s = –0.0685, p = 0.837; Fig. 6d). The

514 Bayes factor gave very strong support to unlinking the clock models between nuclear and
515 floral characters, with an average log Bayes factor of 51.4. Our Bayesian approaches failed to
516 detect a correlation regardless of whether fossil calibrations were included or not (see
517 Supplementary Material for the results of analyses without fossil calibrations).
518
519 ## DISCUSSION
520 We have shown through a comprehensive simulation study that correlated rates of
521 evolution between molecular sequences and morphological characters can be detected under
522 a variety of circumstances. The best-performing method was correlations of Bayesian branch
523 rates, followed by root-to-tip distances, Bayesian model selection, independent sister-pairs
524 contrasts, and lastly likelihood-based model selection. However, when taking computational
525 burden into account, testing for correlations using root-to-tip distances is the most efficient
526 method. Overall, methods had more power when the data had a high degree of among-lineage
527 rate variation, and when at least 45 taxa or 100 morphological characters were sampled.
528 When we applied these methods to an angiosperm data set, we found limited evidence for
529 coupled evolutionary rates when analysing nuclear DNA and floral characters. The estimation
530 of root-to-tip distances might have been misled by missing character data in the floral trait
531 data set. However, missing data are often unavoidable in morphological data sets, due to
532 inapplicable characters, i.e., characters that are not common across species, and difficulties in
533 accessing suitable samples (Scholtz 2010; Wanninger 2015). Although our simulations used
534 evolutionary parameters that were empirically informed, they still represented an idealized
535 form of the evolutionary process and yielded complete data sets. Below we discuss the results
536 and implications of the simulation study before returning to the case study of angiosperms.
537
538

539 *Detecting Correlations Between Rates of Molecular and Morphological Evolution*

540 Our simulation study has provided detailed evaluations of five methods of testing for
541 correlations between rates of molecular and morphological evolution. We found that the three
542 methods that used inferences from maximum-likelihood phylogenetic analysis required at
543 least 100 morphological characters for accurate detection of rate correlations. We found that
544 correlations of root-to-tip distances performed well, with a low rate of false positives. While
545 statistical analyses of root-to-tip distances are hindered by the non-independence of the data
546 points (Rambaut et al. 2016), appropriate *p*-values can be computed using a permutation test
547 (Higgins 2004; Garren 2019). Analysis using independent sister-pair contrasts was able to
548 detect rate correlations less frequently than the other methods that we evaluated, and this is
549 likely to be due to the reduced number of data points that are sampled. For instance, for the
550 tree including 111 species, root-to-tip distance correlations are based on 111 data points,
551 whereas independent sister-pairs contrasts use only 35 data points.

552 When we used likelihood-based model selection to compare models with
553 proportionate (linked) versus unlinked branch lengths, we consistently found support for the
554 proportionate model even for data that had been generated by simulation with uncorrelated
555 rates. However, this was probably because the proportionate model captures a substantial
556 amount of variation while bringing only a modest increase in the number of parameters
557 (Duchêne et al. 2020). The proportionate model was favoured under almost all simulation
558 settings, except when there was a large number of morphological characters. Of the two
559 information criteria that were employed, model selection using the AICc yielded fewer false
560 positives, since it penalizes model size less harshly than the BIC (Duchêne et al. 2020).

561 The two Bayesian methods of testing for rate correlations showed highly contrasting
562 performance in our simulation study. We found that correlations could be detected in our
563 analyses of Bayesian branch rates even under less informative settings, such as when there

were only 10 morphological characters. This strong performance was unexpected, given the typically large uncertainty in estimates of branch rates (e.g., Ho et al. 2005; Drummond et al. 2006), but can perhaps be attributed to the large number of data points sampled by the test (one comparison per branch). Compared with the likelihood-based approach, Bayesian model selection performed well when detecting correlated evolutionary rates, except when there was low among-lineage rate variation. It may be useful to compare the performance of other methods of marginal-likelihood estimation, such as path sampling or nested sampling (Skilling 2006; Russel et al. 2019).

Further evaluations of methods that test for correlations between molecular and morphological rates of evolution will be valuable, given that the dynamics of morphological evolution and the relationship to molecular evolution remain poorly understood (Lee and Palci 2015). In our study, we have not considered processes 'external' to coding in DNA sequences, such as phenotypic plasticity and epigenetics, but these may shape adaptation and phenotypic changes over time (West-Eberhard 1989; Nylin and Wahlberg 2008). Furthermore, there is a lack of congruence between phylogenies inferred from different types of biological data (Oyston et al.), possibly due to the limited size of morphological data sets or the effect of homoplasy (Keating et al. 2020). However, this might not be pertinent at higher taxonomic levels (Jablonski and Finarelli 2009), where diagnostic characters tend to be more informative and can carry strong phylogenetic signal.

By testing for correlations between molecular and morphological evolutionary rates, we can better understand the dynamics of the 'morphological clock'. Whilst a broad link between molecular and morphological change is expected (Simpson 1953), the existence of a morphological clock has so far been rejected (Beck and Lee 2014; Lee and Palci 2015; O'Reilly et al. 2015; Lee 2016; Tarasov 2019). This is reinforced by the apparent lack of a

588 'common mechanism' governing the evolution of morphological characters, with the pattern
589 of among-character rate variation differing across branches (Goloboff et al. 2019).
590 The performance of methods is likely to be worse in analyses of real data sets
591 compared to simulated data sets, because of the complexities of the evolutionary process in
592 reality and because of the shortcomings of our evolutionary models, particularly models of
593 morphological evolution. Estimating morphological rates of evolution is fraught with
594 uncertainty, and the distribution of rates across taxa and over time is largely undescribed
595 (Simpson 1944; Schopf 1984). Unlike molecular data, the collection of morphological data is
596 'infinitely extensible'; there is no upper boundary on the total number of characters and states
597 that can be considered (Oyston et al.), because there are no objectively defined categories
598 such as the 20 amino acids or four nucleotides found in molecular data (Dávalos et al. 2014;
599 Lee and Palci 2015; Barba-Montoya et al. 2021). The morphological characters that are
600 selected for phylogenetic inference are usually chosen for their diagnostic utility, so invariant
601 and rapidly evolving characters are typically excluded (Lewis 2001; Wright and Hillis 2014).
602 Previous work has shown that Bayesian and maximum-parsimony phylogenetic
603 analyses of morphological data have greater accuracy for data that have been generated under
604 stochastic processes rather than being subject to selection (Keating et al. 2020). This indicates
605 that at a macroevolutionary scale, the dynamics of morphological evolution may deviate from
606 the Mk model, which is a simplified version of the general multiple-rate asymmetrical Mk
607 model, originally introduced for morphological data (Pagel 1994; Goloboff et al. 2019;
608 Keating et al. 2020). Although the inadequacy of the Mk model is often assumed to hamper
609 phylogenetic inference using morphological characters, it might not be a substantial problem
610 unless homoplasy is particularly extensive (Jablonski and Finarelli 2009) or when rates are
611 extremely high (Reyes et al. 2018; Klopfstein et al. 2019; Simões et al. 2022a). Apart from
612 these cases, Bayesian inference using the Mk model seems to be relatively robust and can

accurately infer topologies and branch lengths under a broad range of conditions (Klopfstein et al. 2019).

Evolutionary Rates in Angiosperms

Our analysis of data from 111 angiosperms failed to detect a correlation between the evolutionary rates of nuclear DNA and floral traits. The 30-character floral data set that we analysed might not have been sufficiently informative, so our results will require confirmation using larger data sets comprising at least 100 characters. Additionally, the floral data set that we examined excluded hypervariable characters, such as floral colour. The resulting characters in the floral data set were all slowly evolving, at rates below 0.006 changes/Myr. These low rates have been described as 'optimal' for phylogenetic inference (Klopfstein et al. 2019), and were likewise suited to the primary goal of ancestral state reconstruction for which this data set was assembled (Sauquet et al. 2017). However, simulating data sets with a broader diversity of rates, including both higher and lower ones, would be useful. Also, incorporating missing data in the simulations would improve the realism of the data sets and allow evaluation of the impacts of missing data on detecting correlations in evolutionary rates.

The molecular data set used to test for correlations between rates of floral and sequence evolution included 410 protein-coding, single-copy nuclear genes, obtained by sequencing the vegetative tissue transcriptomes of plant species (ONEKP 2019). These 410 protein-coding genes likely control phenotypic expression across a broad range of characters. However, the set of 30 curated floral traits only represents a small proportion of the total phenotypic traits of each flowering plant species. Assessing a larger number of morphological traits will not only lend more power to the analyses but will also provide a more accurate reflection of the overall rate of morphological trait evolution. Such a data set is

not yet available for flowering plants across a broad phylogenetic sample because of the considerable work required in its assembly. Studies could possibly be done with resources such as the global 'TRY' plant database (Kattge et al. 2020), which is composed mostly of vegetative traits. Generally, floral traits are under intense sexual selection (Barrett 2010), which might influence the detection of correlated rates. Indeed, Barraclough and Savolainen (2001) found a very strong correlation between the evolution of molecular sequences and floral traits, but a weak correlation when analysing vegetative traits.

Overall, the result might correctly reflect a more general uncoupling of molecular and morphological rates in angiosperms. A decoupling of evolutionary rates between the nuclear genome and floral characters suggests a departure from a model of gradual morphological change, i.e., that morphological evolution is not proportional to time (Halliday et al. 2019). This may be because the floral characters exhibit high heterogeneity and deviation from clocklike evolution. Indeed, from the Bayesian relaxed-clock analysis, the floral characters exhibited a coefficient of variation of branch rates of 1.53 (95% credible interval 0.896–2.24) whereas the genomic DNA had a coefficient of variation of 1.35 (95% credible interval 1.27–1.52). Pulses of morphological change have occurred throughout plant evolution, possibly at speciation events (Eldredge and Gould 1972), with notable episodes corresponding to the introduction of vascular plants in the Devonian and the diversification of angiosperms in the Late Cretaceous (Leslie et al. 2021).

A lack of an association between rates of floral character and molecular evolution would also be consistent with floral evolution being driven by changes at specific loci (Kimura 1968; Barrier et al. 2001; Davies and Savolainen 2006; Duret 2008; Gaut et al. 2011). The mutations that produce phenotypic change might occur largely in adaptive and regulatory genes, while many genomic mutations are neutral in their impact on fitness (Kimura 1968, 1983). Indeed, a large proportion of the morphological diversity amongst

663 flowering plants can be attributed to specialized interactions between angiosperms and their
664 insect pollinators (Darwin 1862; Friis et al. 2006; Benton et al. 2021; Asar et al. 2022).
665 Furthermore, in our study, we were limited to examining evolutionary change in protein-
666 coding genes, which only included the first two sites of each codon. Testing for correlations
667 separately using rates of nonsynonymous and synonymous substitution will allow further
668 insights into the relative importance of selection and drift (Barrier et al. 2001).
669
670 *Concluding Remarks*
671 We have shown that correlations between molecular and morphological evolutionary
672 rates can be detected under the conditions explored in our simulation study. However, the
673 complexities of how morphological evolution proceeds, and whether this is effectively
674 described by current evolutionary models and approaches, will ultimately determine whether
675 the rates of morphological character evolution and their correlates can be accurately
676 reconstructed in practice. While we did not find evidence of correlated evolutionary rates
677 between angiosperm genomic DNA and floral characters, the question of whether the rates of
678 genotypic and phenotypic evolution are correlated in angiosperms should be addressed with a
679 larger morphological data set.
680 Our study has implications for combined analyses of molecular and morphological
681 data, where branch lengths between data sets are often linked as a default approach (Nylander
682 et al. 2004; O'Reilly et al. 2015). The results of our simulation study lead us to suggest that
683 future studies should use morphological character matrices of at least 100 characters; this
684 would allow for partitioning of the morphological data set, which has been demonstrated to
685 improve the precision of divergence date estimates and accuracy of branch-length estimates
686 (Lee 2016; Caldas and Schrago 2019; Neumann et al. 2021). Moreover, increasing the size of
687 the morphological data set can minimize the impacts of character correlation (Guillerme and

688 Brazeau 2018; Simões et al. 2022a). This work should not only be extended to larger data
689 sets, but should also span across the Tree of Life, to help elucidate the processes that drive
690 macroevolutionary change. Furthermore, these methods are not restricted to analyses of
691 molecular and morphological evolution, but can also be used to test for correlations in rates
692 between symbionts and their hosts or between organellar and nuclear genomes in plants.
693
694 ## SUPPLEMENTARY MATERIALS
695 Supplementary material is available online. All text, files and code are available at Dryad
696 [X].
697
698 ## ACKNOWLEDGEMENTS
699 Y.A. acknowledges the support provided by the Australian Government's Research Training
700 Program award. This work was funded by the Australian Research Council (DP220103265).
701 The authors acknowledge the Sydney Informatics Hub and the high-performance computing
702 facility, Artemis, at the University of Sydney for providing computing resources.

REFERENCES

703 Ackermann R.R., Cheverud J.M. 2004. Detecting genetic drift versus selection in human
704 evolution. Proc. Natl. Acad. Sci. U. S. A. 101:17946–17951.
705 Amemiya C.T., Alfoldi J., Lee A.P., Fan S., Philippe H., MacCallum I., Braasch I.,
706 Manousaki T., Schneider I., Rohner N., Organ C., Chalopin D., Smith J.J., Robinson M.,
707 Dorrington R.A., Gerdol M., Aken B., Biscotti M.A., Barucca M., Baurain D., Berlin
708 A.M., Blatch G.L., Buonocore F., Burmester T., Campbell M.S., Canapa A., Cannon
709 J.P., Christoffels A., De Moro G., Edkins A.L., Fan L., Fausto A.M., Feiner N., Forconi
710 M., Gamieldien J., Gnerre S., Gnirke A., Goldstone J. V., Haerty W., Hahn M.E., Hesse
711 U., Hoffmann S., Johnson J., Karchner S.I., Kuraku S., Lara M., Levin J.Z., Litman
712 G.W., Mauceli E., Miyake T., Mueller M.G., Nelson D.R., Nitsche A., Olmo E., Ota T.,
713 Pallavicini A., Panji S., Picone B., Ponting C.P., Prohaska S.J., Przybylski D., Saha
714 N.R., Ravi V., Ribeiro F.J., Sauka-Spengler T., Scapigliati G., Searle S.M.J., Sharpe T.,
715 Simakov O., Stadler P.F., Stegeman J.J., Sumiyama K., Tabbaa D., Tafer H., Turner-
716 Maier J., Van Heusden P., White S., Williams L., Yandell M., Brinkmann H., Volff J.N.,
717 Tabin C.J., Shubin N., Schartl M., Jaffe D.B., Postlethwait J.H., Venkatesh B., Di Palma
718 F., Lander E.S., Meyer A., Lindblad-Toh K. 2013. The African coelacanth genome
719 provides insights into tetrapod evolution. Nature. 496:311–316.
720 Anderson S.A.S., Weir J.T. 2022. diverge: Evolutionary Trait Divergence Between Sister
721 Species and Other Paired Lineages. R Package. version 2.0.4.
722 Arab D.A., Bourguignon T., Wang Z., Ho S.Y.W., Lo N. 2020. Evolutionary rates are
723 correlated between cockroach symbionts and mitochondrial genomes. Biol Lett.
724 16:20190702.
725 Asar Y., Ho S.Y.W., Sauquet H. 2022. Early diversifications of angiosperms and their insect
726 pollinators: Were they unlinked? Trends Plant Sci. (in press).

727 Ashton D.T., Ritchie P.A., Wellenreuther M. 2017. Fifteen years of quantitative trait loci
728 studies in fish: challenges and future directions. Mol. Ecol. 26:1465–1476.
729 Avise J.C., Nelson W.S., Sugita H. 1994. A speciational history of "living fossils'':
730 molecular evolutionary patterns in horseshoe crabs." Evolution. 48:1986–2001.
731 Baele G., Lemey P., Suchard M.A. 2016. Genealogical working distributions for Bayesian
732 model testing with phylogenetic uncertainty. Syst. Biol. 65:250–264.
733 Barba-Montoya J., Tao Q., Kumar S. 2021. Molecular and morphological clocks for
734 estimating evolutionary divergence times. BMC Ecol. Evol. 21:1–15.
735 Barraclough T.G., Savolainen V. 2001. Evolutionary rates and species diversity in flowering
736 plants. Evolution. 55:677–683.
737 Barrett S.C.H. 2010. Darwin's legacy: The forms, function and sexual diversity of flowers.
738 Philos. Trans. R. Soc. B Biol. Sci. 365:351–368.
739 Barrier M., Robichaux R.H., Purugganan M.D. 2001. Accelerated regulatory gene evolution
740 in an adaptive radiation. Proc. Natl. Acad. Sci. U. S. A. 98:10208–10213.
741 Beck R.M.D., Lee M.S.Y. 2014. Ancient dates or accelerated rates? Morphological clocks
742 and the antiquity of placental mammals. Proc. R. Soc. B Biol. Sci. 281.
743 Benton M., Wilf P., Sauquet H. 2021. The angiosperm terrestrial revolution and the origins of
744 modern biodiversity. New Phytol. 223:2017–2035.
745 Bouckaert R., Vaughan T.G., Barido-Sottani J., Duchêne S., Fourment M., Gavryushkina A.,
746 Heled J., Jones G., Kühnert D., De Maio N., Matschiner M., Mendes F.K., Müller N.F.,
747 Ogilvie H.A., du Plessis L., Popinga A., Rambaut A., Rasmussen D., Siveroni I.,
748 Suchard M.A., Wu C.-H., Xie D., Zhang C., Stadler T., Drummond A.J. 2019. BEAST
749 2.5: An advanced software platform for Bayesian evolutionary analysis. PLOS Comput.
750 Biol. 15:e1006650.
751 Bromham L., Woolfit M., Lee M.S.Y., Rambaut A. 2002. Testing the relationship between

752 morphological and molecular rates of change along phylogenies. Evolution. 56:1921–
753 1930.
754 Bui M.Q., Schmidt H.A., Chernomor O., Schrempf D., Woodhams M.D., von Haeseler A.,
755 Lanfear R. 2020. IQ-TREE 2: New Models and Efficient Methods for Phylogenetic
756 Inference in the Genomic Era. Mol. Biol. Evol. 37:1530–1534.
757 Caldas I. V., Schrago C.G. 2019. Data partitioning and correction for ascertainment bias
758 reduce the uncertainty of placental mammal divergence times inferred from the
759 morphological clock. Ecol. Evol. 9:2255–2262.
760 Cappellari S.C., Schaefer H., Davis C.C. 2013. Evolution: pollen or pollinators - which came
761 first? Curr Biol. 23:316–318.
762 Combosch D.J., Lemer S., Ward P.D., Landman N.H., Giribet G. 2017. Genomic signatures
763 of evolution in Nautilus—An endangered living fossil. Mol. Ecol. 26:5923–5938.
764 Darwin C. 1862. On the various contrivances by which British and foreign orchids are
765 fertilised by insects, and on the good effects of intercrossing. London, UK: John Murray.
766 Dávalos L.M., Velazco P.M., Warsi O.M., Smits P.D., Simmons N.B. 2014. Integrating
767 incomplete fossils by isolating conflicting signal in saturated and non-independent
768 morphological characters. Syst. Biol. 63:582–600.
769 Davies T.J., Savolainen V. 2006. Neutral theory, phylogenies, and the relationship between
770 phenotypic change and evolutionary rates. Evolution. 60:476–483.
771 Drummond A.J., Ho S.Y.W., Phillips M.J., Rambaut A. 2006. Relaxed Phylogenetics and
772 Dating with Confidence. PLOS Biol. 4:e88.
773 Duchêne D.A., Tong K.J., Foster C.S.P., Duchêne S., Lanfear R., Ho S.Y.W. 2020. Linking
774 branch lengths across sets of loci provides the highest statistical support for phylogenetic
775 inference. Mol. Biol. Evol. 37:1202–1210.
776 Duret L. 2008. The null hypothesis of molecular evolution. Nat. Educ. 1:218.

777 Eldredge N., Gould S. 1972. Punctuated equilibria: an alternative to phyletic gradualism. In:
778 Schopf T., editor. Models in Paleobiology. Freeman Cooper. p. 82–115.
779 Felsenstein J. 1985. Phylogenies and the Comparative Method. Am. Nat. 125:1–15.
780 Freckleton R.P. 2000. Phylogenetic tests of ecological and evolutionary hypotheses: checking
781 for phylogenetic independence. Funct. Ecol. 14:129–134.
782 Friis E.M., Pedersen K.R., Crane P.R. 2006. Cretaceous angiosperm flowers: Innovation and
783 evolution in plant reproduction. Palaeogeogr. Palaeoclimatol. Palaeoecol. 232:251–293.
784 Garland T., Harvey P.H., Ives A.R. 1992. Procedures for the analysis of comparative data
785 using phylogenetically independent contrasts. Syst. Biol. 41:18–32.
786 Garren S.T. 2019. jmuOutlier: Permutation Tests for Nonparametric Statistics. R package
787 version 2.2.
788 Gaut B., Yang L., Takuno S., Eguiarte L.E. 2011. The Patterns and Causes of Variation in
789 Plant Nucleotide Substitution Rates. Annu. Rev. Ecol. Evol. Syst. 42:245–266.
790 Gemmell N.J., Rutherford K., Prost S., Tollis M., Winter D., Macey J.R., Adelson D.L., Suh
791 A., Bertozzi T., Grau J.H., Organ C., Gardner P.P., Muffato M., Patricio M., Billis K.,
792 Martin F.J., Flicek P., Petersen B., Kang L., Michalak P., Buckley T.R., Wilson M.,
793 Cheng Y., Miller H., Schott R.K., Jordan M.D., Newcomb R.D., Arroyo J.I., Valenzuela
794 N., Hore T.A., Renart J., Peona V., Peart C.R., Warmuth V.M., Zeng L., Kortschak
795 R.D., Raison J.M., Zapata V.V., Wu Z., Santesmasses D., Mariotti M., Guigó R., Rupp
796 S.M., Twort V.G., Dussex N., Taylor H., Abe H., Bond D.M., Paterson J.M., Mulcahy
797 D.G., Gonzalez V.L., Barbieri C.G., DeMeo D.P., Pabinger S., Van Stijn T., Clarke S.,
798 Ryder O., Edwards S. V., Salzberg S.L., Anderson L., Nelson N., Stone C., Stone C.,
799 Smillie J., Edmonds H. 2020. The tuatara genome reveals ancient features of amniote
800 evolution. Nature. 584:403–409.
801 Gillespie J.H. 1991. The causes of molecular evolution. Oxford, United Kingdom: Oxford

802 University Press.
803 Goloboff P.A., Pittman M., Pol D., Xu X. 2019. Morphological data sets fit a common
804 mechanism much more poorly than DNA sequences and call into question the Mkv
805 model. Syst Biol. 68:494–504.
806 Gould S.J., Eldredge N. 1977. Punctuated equilibria: the tempo and mode of evolution
807 reconsidered. Paleobiology. 3:115–151.
808 Guan R., Zhao Y., Zhang H., Fan G., Liu X., Zhou W., Shi C., Wang J., Liu W., Liang X., Fu
809 Y., Ma K., Zhao L., Zhang F., Lu Z., Lee S.M.Y., Xu X., Wang J., Yang H., Fu C., Ge
810 S., Chen W. 2016. Draft genome of the living fossil *Ginkgo biloba*. Gigascience. 5:49.
811 Guillerme T., Brazeau M.D. 2018. Influence of different modes of morphological character
812 correlation on phylogenetic tree inference. bioRxiv. 308742.
813 Halliday T.J.D., Dos Reis M., Tamuri A.U., Ferguson-Gow H., Yang Z., Goswami A. 2019.
814 Rapid morphological evolution in placental mammals post-dates the origin of the crown
815 group. Proc. R. Soc. B Biol. Sci. 286:20182418.
816 Hay J.M., Subramanian S., Millar C.D., Mohandesan E., Lambert D.M. 2008. Rapid
817 molecular evolution in a living fossil. Trends Genet. 24:106–109.
818 Herrera-Flores J.A., Stubbs T.L., Benton M.J. 2017. Macroevolutionary patterns in
819 Rhynchocephalia: is the tuatara (Sphenodon punctatus) a living fossil? Palaeontology.
820 60:319–328.
821 Higgins J.J. 2004. Introduction to Modern Nonparametric Statistics. Thomson, Brooks/Cole.
822 Ho S.Y.W., Phillips M.J. 2009. Accounting for calibration uncertainty in phylogenetic
823 estimation of evolutionary divergence times. Syst. Biol. 58:367–380.
824 Ho S.Y.W., Duchêne S., Duchêne D. 2015. Simulating and detecting autocorrelation of
825 molecular evolutionary rates among lineages. Mol. Ecol. Resour. 15:688–696.
826 Ho S.Y.W., Phillips M.J., Drummond A.J., Cooper A. 2005. Accuracy of rate estimation

using relaxed-clock models with a critical focus on the early metazoan radiation. Mol. Biol. Evol. 22:1355–1363.

Ho W.C., Ohya Y., Zhang J. 2017. Testing the neutral hypothesis of phenotypic evolution. Proc. Natl. Acad. Sci. U. S. A. 114:12219–12224.

Huang Z., Huang W., Liu X., Han Z., Liu G., Boamah G.A., Wang Y., Yu F., Gan Y., Xiao Q., Luo X., Chen N., Liu M., You W., Ke C. 2022. Genomic insights into the adaptation and evolution of the nautilus, an ancient but evolving "living fossil." Mol. Ecol. Resour. 22:15–27.

Jablonski D., Finarelli J. 2009. Congruence of morphologically-defined genera with molecular phylogenies. Proc. Natl. Acad. Sci. U. S. A.:8262.

Jombart T., Balloux F., Dray S. 2010. adephylo: new tools for investigating the phylogenetic signal in biological traits. Bioinformatics. 26:1907–1909.

Jukes T.H., Cantor C.R. 1969. Evolution of Protein Molecules. New York: Academic Press.

Kalyaanamoorthy S., Minh B.Q., Wong T.K.F., von Haeseler A., Jermiin L.S. 2017. ModelFinder: fast model selection for accurate phylogenetic estimates. Nat. Methods. 14:587–589.

Kass R.E., Raftery A.E. 1995. Bayes Factors. J. Am. Stat. Assoc. 90:773–795.

Kattge J., Bönisch G., Díaz S., Lavorel S., Prentice I.C., Leadley P., Tautenhahn S., Werner G.D.A., Aakala T., Abedi M., Acosta A.T.R., Adamidis G.C., Adamson K., Aiba M., Albert C.H., Alcántara J.M., Alcázar C C., Aleixo I., Ali H., Amiaud B., Ammer C., Amoroso M.M., Anand M., Anderson C., Anten N., Antos J., Apgaua D.M.G., Ashman T.-L., Asmara D.H., Asner G.P., Aspinwall M., Atkin O., Aubin I., Baastrup-Spohr L., Bahalkeh K., Bahn M., Baker T., Baker W.J., Bakker J.P., Baldocchi D., Baltzer J., Banerjee A., Baranger A., Barlow J., Barneche D.R., Baruch Z., Bastianelli D., Battles J., Bauerle W., Bauters M., Bazzato E., Beckmann M., Beeckman H., Beierkuhnlein C.,

852 Bekker R., Belfry G., Belluau M., Beloiu M., Benavides R., Benomar L., Berdugo-
853 Lattke M.L., Berenguer E., Bergamin R., Bergmann J., Bergmann Carlucci M., Berner
854 L., Bernhardt-Römermann M., Bigler C., Bjorkman A.D., Blackman C., Blanco C.,
855 Blonder B., Blumenthal D., Bocanegra-González K.T., Boeckx P., Bohlman S.,
856 Böhning-Gaese K., Boisvert-Marsh L., Bond W., Bond-Lamberty B., Boom A.,
857 Boonman C.C.F., Bordin K., Boughton E.H., Boukili V., Bowman D.M.J.S., Bravo S.,
858 Brendel M.R., Broadley M.R., Brown K.A., Bruelheide H., Brumnich F., Bruun H.H.,
859 Bruy D., Buchanan S.W., Bucher S.F., Buchmann N., Buitenwerf R., Bunker D.E.,
860 Bürger J., Burrascano S., Burslem D.F.R.P., Butterfield B.J., Byun C., Marques M.,
861 Scalon M.C., Caccianiga M., Cadotte M., Cailleret M., Camac J., Camarero J.J.,
862 Campany C., Campetella G., Campos J.A., Cano-Arboleda L., Canullo R., Carbognani
863 M., Carvalho F., Casanoves F., Castagneyrol B., Catford J.A., Cavender-Bares J.,
864 Cerabolini B.E.L., Cervellini M., Chacón-Madrigal E., Chapin K., Chapin F.S., Chelli
865 S., Chen S.-C., Chen A., Cherubini P., Chianucci F., Choat B., Chung K.-S., Chytrý M.,
866 Ciccarelli D., Coll L., Collins C.G., Conti L., Coomes D., Cornelissen J.H.C., Cornwell
867 W.K., Corona P., Coyea M., Craine J., Craven D., Cromsigt J.P.G.M., Csecserits A.,
868 Cufar K., Cuntz M., da Silva A.C., Dahlin K.M., Dainese M., Dalke I., Dalle Fratte M.,
869 Dang-Le A.T., Danihelka J., Dannoura M., Dawson S., de Beer A.J., De Frutos A., De
870 Long J.R., Dechant B., Delagrange S., Delpierre N., Derroire G., Dias A.S., Diaz-
871 Toribio M.H., Dimitrakopoulos P.G., Dobrowolski M., Doktor D., Dřevojan P., Dong
872 N., Dransfield J., Dressler S., Duarte L., Ducouret E., Dullinger S., Durka W., Duursma
873 R., Dymova O., E-Vojtkó A., Eckstein R.L., Ejtehadi H., Elser J., Emilio T., Engemann
874 K., Erfanian M.B., Erfmeier A., Esquivel-Muelbert A., Esser G., Estiarte M.,
875 Domingues T.F., Fagan W.F., Fagúndez J., Falster D.S., Fan Y., Fang J., Farris E.,
876 Fazlioglu F., Feng Y., Fernandez-Mendez F., Ferrara C., Ferreira J., Fidelis A., Finegan

877 B., Firn J., Flowers T.J., Flynn D.F.B., Fontana V., Forey E., Forgiarini C., François L.,
878 Frangipani M., Frank D., Frenette-Dussault C., Freschet G.T., Fry E.L., Fyllas N.M.,
879 Mazzochini G.G., Gachet S., Gallagher R., Ganade G., Ganga F., García-Palacios P.,
880 Gargaglione V., Garnier E., Garrido J.L., de Gasper A.L., Gea-Izquierdo G., Gibson D.,
881 Gillison A.N., Giroldo A., Glasenhardt M.-C., Gleason S., Gliesch M., Goldberg E.,
882 Göldel B., Gonzalez-Akre E., Gonzalez-Andujar J.L., González-Melo A., González-
883 Robles A., Graae B.J., Granda E., Graves S., Green W.A., Gregor T., Gross N., Guerin
884 G.R., Günther A., Gutiérrez A.G., Haddock L., Haines A., Hall J., Hambuckers A., Han
885 W., Harrison S.P., Hattingh W., Hawes J.E., He T., He P., Heberling J.M., Helm A.,
886 Hempel S., Hentschel J., Hérault B., Hereş A.-M., Herz K., Heuertz M., Hickler T.,
887 Hietz P., Higuchi P., Hipp A.L., Hirons A., Hock M., Hogan J.A., Holl K., Honnay O.,
888 Hornstein D., Hou E., Hough-Snee N., Hovstad K.A., Ichie T., Igić B., Illa E., Isaac M.,
889 Ishihara M., Ivanov L., Ivanova L., Iversen C.M., Izquierdo J., Jackson R.B., Jackson
890 B., Jactel H., Jagodzinski A.M., Jandt U., Jansen S., Jenkins T., Jentsch A., Jespersen
891 J.R.P., Jiang G.-F., Johansen J.L., Johnson D., Jokela E.J., Joly C.A., Jordan G.J.,
892 Joseph G.S., Junaedi D., Junker R.R., Justes E., Kabzems R., Kane J., Kaplan Z.,
893 Kattenborn T., Kavelenova L., Kearsley E., Kempel A., Kenzo T., Kerkhoff A., Khalil
894 M.I., Kinlock N.L., Kissling W.D., Kitajima K., Kitzberger T., Kjøller R., Klein T.,
895 Kleyer M., Klimešová J., Klipel J., Kloeppel B., Klotz S., Knops J.M.H., Kohyama T.,
896 Koike F., Kollmann J., Komac B., Komatsu K., König C., Kraft N.J.B., Kramer K.,
897 Kreft H., Kühn I., Kumarathunge D., Kuppler J., Kurokawa H., Kurosawa Y., Kuyah S.,
898 Laclau J.-P., Lafleur B., Lallai E., Lamb E., Lamprecht A., Larkin D.J., Laughlin D., Le
899 Bagousse-Pinguet Y., le Maire G., le Roux P.C., le Roux E., Lee T., Lens F., Lewis S.L.,
900 Lhotsky B., Li Y., Li X., Lichstein J.W., Liebergesell M., Lim J.Y., Lin Y.-S., Linares
901 J.C., Liu C., Liu D., Liu U., Livingstone S., Llusià J., Lohbeck M., López-García Á.,

902 Lopez-Gonzalez G., Lososová Z., Louault F., Lukács B.A., Lukeš P., Luo Y., Lussu M.,
903 Ma S., Maciel Rabelo Pereira C., Mack M., Maire V., Mäkelä A., Mäkinen H., Malhado
904 A.C.M., Mallik A., Manning P., Manzoni S., Marchetti Z., Marchino L., Marcilio-Silva
905 V., Marcon E., Marignani M., Markesteijn L., Martin A., Martínez-Garza C., Martínez-
906 Vilalta J., Mašková T., Mason K., Mason N., Massad T.J., Masse J., Mayrose I.,
907 McCarthy J., McCormack M.L., McCulloh K., McFadden I.R., McGill B.J., McPartland
908 M.Y., Medeiros J.S., Medlyn B., Meerts P., Mehrabi Z., Meir P., Melo F.P.L.,
909 Mencuccini M., Meredieu C., Messier J., Mészáros I., Metsaranta J., Michaletz S.T.,
910 Michelaki C., Migalina S., Milla R., Miller J.E.D., Minden V., Ming R., Mokany K.,
911 Moles A.T., Molnár V A., Molofsky J., Molz M., Montgomery R.A., Monty A.,
912 Moravcová L., Moreno-Martínez A., Moretti M., Mori A.S., Mori S., Morris D.,
913 Morrison J., Mucina L., Mueller S., Muir C.D., Müller S.C., Munoz F., Myers-Smith
914 I.H., Myster R.W., Nagano M., Naidu S., Narayanan A., Natesan B., Negoita L., Nelson
915 A.S., Neuschulz E.L., Ni J., Niedrist G., Nieto J., Niinemets Ü., Nolan R., Nottebrock
916 H., Nouvellon Y., Novakovskiy A., Network T.N., Nystuen K.O., O'Grady A., O'Hara
917 K., O'Reilly-Nugent A., Oakley S., Oberhuber W., Ohtsuka T., Oliveira R., Öllerer K.,
918 Olson M.E., Onipchenko V., Onoda Y., Onstein R.E., Ordonez J.C., Osada N., Ostonen
919 I., Ottaviani G., Otto S., Overbeck G.E., Ozinga W.A., Pahl A.T., Paine C.E.T.,
920 Pakeman R.J., Papageorgiou A.C., Parfionova E., Pärtel M., Patacca M., Paula S., Paule
921 J., Pauli H., Pausas J.G., Peco B., Penuelas J., Perea A., Peri P.L., Petisco-Souza A.C.,
922 Petraglia A., Petritan A.M., Phillips O.L., Pierce S., Pillar V.D., Pisek J., Pomogaybin
923 A., Poorter H., Portsmuth A., Poschlod P., Potvin C., Pounds D., Powell A.S., Power
924 S.A., Prinzing A., Puglielli G., Pyšek P., Raevel V., Rammig A., Ransijn J., Ray C.A.,
925 Reich P.B., Reichstein M., Reid D.E.B., Réjou-Méchain M., de Dios V.R., Ribeiro S.,
926 Richardson S., Riibak K., Rillig M.C., Riviera F., Robert E.M.R., Roberts S., Robroek

927 B., Roddy A., Rodrigues A.V., Rogers A., Rollinson E., Rolo V., Römermann C.,
928 Ronzhina D., Roscher C., Rosell J.A., Rosenfield M.F., Rossi C., Roy D.B., Royer-
929 Tardif S., Rüger N., Ruiz-Peinado R., Rumpf S.B., Rusch G.M., Ryo M., Sack L.,
930 Saldaña A., Salgado-Negret B., Salguero-Gomez R., Santa-Regina I., Santacruz-García
931 A.C., Santos J., Sardans J., Schamp B., Scherer-Lorenzen M., Schleuning M., Schmid
932 B., Schmidt M., Schmitt S., Schneider J. V, Schowanek S.D., Schrader J., Schrodt F.,
933 Schuldt B., Schurr F., Selaya Garvizu G., Semchenko M., Seymour C., Sfair J.C.,
934 Sharpe J.M., Sheppard C.S., Sheremetiev S., Shiodera S., Shipley B., Shovon T.A.,
935 Siebenkäs A., Sierra C., Silva V., Silva M., Sitzia T., Sjöman H., Slot M., Smith N.G.,
936 Sodhi D., Soltis P., Soltis D., Somers B., Sonnier G., Sørensen M.V., Sosinski Jr E.E.,
937 Soudzilovskaia N.A., Souza A.F., Spasojevic M., Sperandii M.G., Stan A.B., Stegen J.,
938 Steinbauer K., Stephan J.G., Sterck F., Stojanovic D.B., Strydom T., Suarez M.L.,
939 Svenning J.-C., Svitková I., Svitok M., Svoboda M., Swaine E., Swenson N., Tabarelli
940 M., Takagi K., Tappeiner U., Tarifa R., Tauugourdeau S., Tavsanoglu C., te Beest M.,
941 Tedersoo L., Thiffault N., Thom D., Thomas E., Thompson K., Thornton P.E., Thuiller
942 W., Tichý L., Tissue D., Tjoelker M.G., Tng D.Y.P., Tobias J., Török P., Tarin T.,
943 Torres-Ruiz J.M., Tóthmérész B., Treurnicht M., Trivellone V., Trolliet F., Trotsiuk V.,
944 Tsakalos J.L., Tsiripidis I., Tysklind N., Umehara T., Usoltsev V., Vadeboncoeur M.,
945 Vaezi J., Valladares F., Vamosi J., van Bodegom P.M., van Breugel M., Van Cleemput
946 E., van de Weg M., van der Merwe S., van der Plas F., van der Sande M.T., van Kleunen
947 M., Van Meerbeek K., Vanderwel M., Vanselow K.A., Vårhammar A., Varone L.,
948 Vasquez Valderrama M.Y., Vassilev K., Vellend M., Veneklaas E.J., Verbeeck H.,
949 Verheyen K., Vibrans A., Vieira I., Villacís J., Violle C., Vivek P., Wagner K., Waldram
950 M., Waldron A., Walker A.P., Waller M., Walther G., Wang H., Wang F., Wang W.,
951 Watkins H., Watkins J., Weber U., Weedon J.T., Wei L., Weigelt P., Weiher E., Wells

952 A.W., Wellstein C., Wenk E., Westoby M., Westwood A., White P.J., Whitten M.,
953 Williams M., Winkler D.E., Winter K., Womack C., Wright I.J., Wright S.J., Wright J.,
954 Pinho B.X., Ximenes F., Yamada T., Yamaji K., Yanai R., Yankov N., Yguel B., Zanini
955 K.J., Zanne A.E., Zelený D., Zhao Y.-P., Zheng J., Zheng J., Ziemińska K., Zirbel C.R.,
956 Zizka G., Zo-Bi I.C., Zotz G., Wirth C. 2020. TRY plant trait database – enhanced
957 coverage and open access. Glob. Chang. Biol. 26:119–188.
958 Keating J.N., Sansom R.S., Sutton M.D., Knight C.G., Garwood R.J. 2020. Morphological
959 Phylogenetics Evaluated Using Novel Evolutionary Simulations. Syst. Biol. 69:897–
960 912.
961 Kemble H., Nghe P., Tenaillon O. 2019. Recent insights into the genotype–phenotype
962 relationship from massively parallel genetic assays. Evol. Appl. 12:1721–1742.
963 Kimura M. 1968. Evolutionary Rate at the Molecular Level. Nature. 217:624–626.
964 Kimura M. 1983. The Neutral Theory of Molecular Evolution. Cambridge: Cambridge
965 University Press.
966 Klopfstein S., Ryer R., Coiro M., Spasojevic T. 2019. Mismatch of the morphology model is
967 mostly unproblematic in total-evidence dating: insights from an extensive simulation
968 study. bioRxiv. 679084.
969 Lee M.S. 2016. Multiple morphological clocks and total-evidence tip-dating in mammals.
970 Biol Lett. 12. 20160033.
971 Lee M.S., Palci A. 2015. Morphological Phylogenetics in the Genomic Age. Curr Biol. 25:
972 922-929.
973 Lee M.S., Soubrier J., Edgecombe G.D. 2013. Rates of phenotypic and genomic evolution
974 during the Cambrian explosion. Curr Biol. 23:1889–1895.
975 Leslie A.B., Simpson C., Mander L. 2021. Reproductive innovations and pulsed rise in plant
976 complexity. Science. 373:1368–1372.

977 Lewis P.O. 2001. A likelihood approach to estimating phylogeny from discrete
978 morphological character data. Syst. Biol. 50:913–925.
979 Lidgard S., Love A.C. 2018. Rethinking living fossils. Bioscience. 68:760–770.
980 Magallón S., Gomez-Acevedo S., Sanchez-Reyes L.L., Hernandez-Hernandez T. 2015. A
981 metacalibrated time-tree documents the early rise of flowering plant phylogenetic
982 diversity. New Phytol. 207:437–453.
983 Manceau M., Marin J., Morlon H., Lambert A. 2020. Model-Based Inference of Punctuated
984 Molecular Evolution. Mol. Biol. Evol. 37:3308–3323.
985 Ming R., VanBuren R., Liu Y., Yang M., Han Y., Li L.T., Zhang Q., Kim M.J., Schatz M.C.,
986 Campbell M., Li J., Bowers J.E., Tang H., Lyons E., Ferguson A.A., Narzisi G., Nelson
987 D.R., Blaby-Haas C.E., Gschwend A.R., Jiao Y., Der J.P., Zeng F., Han J., Min X.J.,
988 Hudson K.A., Singh R., Grennan A.K., Karpowicz S.J., Watling J.R., Ito K., Robinson
989 S.A., Hudson M.E., Yu Q., Mockler T.C., Carroll A., Zheng Y., Sunkar R., Jia R., Chen
990 N., Arro J., Wai C.M., Wafula E., Spence A., Han Y., Xu L., Zhang J., Peery R., Haus
991 M.J., Xiong W., Walsh J.A., Wu J., Wang M.L., Zhu Y.J., Paull R.E., Britt A.B., Du C.,
992 Downie S.R., Schuler M.A., Michael T.P., Long S.P., Ort D.R., William Schopf J.,
993 Gang D.R., Jiang N., Yandell M., dePamphilis C.W., Merchant S.S., Paterson A.H.,
994 Buchanan B.B., Li S., Shen-Miller J. 2013. Genome of the long-living sacred lotus
995 (Nelumbo nucifera Gaertn.). Genome Biol. 14:R41.
996 Neumann J.S., Desalle R., Narechania A., Schierwater B., Tessler M. 2021. Morphological
997 characters can strongly influence early animal relationships inferred from phylogenomic
998 data sets. Syst. Biol. 70:360–375.
999 Nylander J.A.A., Ronquist F., Huelsenbeck J.P., Nieves-Aldrey J.L. 2004. Bayesian
1000 phylogenetic analysis of combined data. Syst. Biol. 53:47–67.
1001 Nylin S., Wahlberg N. 2008. Does plasticity drive speciation? Host-plant shifts and

1002 diversification in nymphaline butterflies (Lepidoptera: Nymphalidae) during the tertiary.
1003 Biol. J. Linn. Soc. 94:115–130.
1004 O'Reilly J.E., dos Reis M., Donoghue P.C.J. 2015. Dating Tips for Divergence-Time
1005 Estimation. Trends Genet. 31:637–650.
1006 Ohta T. 1992. The Nearly Neutral Theory of Molecular Evolution. Annu. Rev. Ecol. Syst.
1007 23:263–286.
1008 Omland K.E. 1997. Correlated rates of molecular and morphological evolution. Evolution.
1009 51:1381–1393.
1010 One Thousand Plant Transcriptomes Initiative. 2019. One thousand plant transcriptomes and
1011 the phylogenomics of green plants. Nature. 574:679–685.
1012 Onstein R.E. 2019. Darwin's second "abominable mystery": trait flexibility as the innovation
1013 leading to angiosperm diversity. New Phytol. DOI: 10.1111/nph.16294
1014 Orr A. 2001. The genetics of species differences. Trends Ecol. Evol. 16:343–350.
1015 Oyston J.W., Wilkinson M., Ruta M., Wills M.A. Molecular phylogenies map to
1016 biogeography better than morphological ones. 5:521.
1017 Pagel M. 1994. Detecting correlated evolution on phylogenies: a general method for the
1018 comparative analysis of discrete characters. Proc. R. Soc. Lond. B. 255:37–45.
1019 Pennell M.W., Eastman J.M., Slater G.J., Brown J.W., Uyeda J.C., FitzJohn R.G., Alfaro
1020 M.E., Harmon L.J. 2014. geiger v2.0: an expanded suite of methods for fitting
1021 macroevolutionary models to phylogenetic trees. Bioinformatics. 30:2216–2218.
1022 Rambaut A., Grass N.C. 1997. Seq-Gen: an application for the Monte Carlo simulation of
1023 DNA sequence evolution along phylogenetic trees. Bioinformatics. 13:235–238.
1024 Rambaut A., Lam T.T., Max Carvalho L., Pybus O.G. 2016. Exploring the temporal structure
1025 of heterochronous sequences using TempEst (formerly Path-O-Gen). Virus Evol.
1026 2:vew007.

1027 Ramírez-Barahona S., Sauquet H., Magallón S. 2020. The delayed and geographically
1028 heterogeneous diversification of flowering plant families. Nat. Ecol. Evol. 4:1232–1238.
1029 Renaud S., Chevret P., Michaux J. 2007. Morphological vs. molecular evolution: ecology and
1030 phylogeny both shape the mandible of rodents. Zool. Scr. 36:525–535.
1031 Reyes E., Nadot S., von Balthazar M., Schonenberger J., Sauquet H. 2018. Testing the impact
1032 of morphological rate heterogeneity on ancestral state reconstruction of five floral traits
1033 in angiosperms. Sci Rep. 8:9473.
1034 Russel P.M., Brewer B.J., Klaere S., Bouckaert R.R. 2019. Model selection and parameter
1035 inference in phylogenetics using nested sampling. Syst. Biol. 68:219–233.
1036 Sanchez G., Simakov O., S Rokhsar D. 2022. Beyond "living fossils": Can comparative
1037 genomics finally reveal novelty? Mol. Ecol. Resour. 22:9–11.
1038 Sauquet H., von Balthazar M., Magallon S., Doyle J.A., Endress P.K., Bailes E.J., Barroso de
1039 Morais E., Bull-Herenu K., Carrive L., Chartier M., Chomicki G., Coiro M., Cornette
1040 R., El Ottra J.H.L., Epicoco C., Foster C.S.P., Jabbour F., Haevermans A., Haevermans
1041 T., Hernandez R., Little S.A., Lofstrand S., Luna J.A., Massoni J., Nadot S., Pamperl S.,
1042 Prieu C., Reyes E., Dos Santos P., Schoonderwoerd K.M., Sontag S., Soulebeau A.,
1043 Staedler Y., Tschan G.F., Wing-Sze Leung A., Schonenberger J. 2017. The ancestral
1044 flower of angiosperms and its early diversification. Nat Commun. 8:16047.
1045 Sauquet H., Magallon S. 2018. Key questions and challenges in angiosperm macroevolution.
1046 New Phytol. 219:1170–1187.
1047 Scholtz G. 2010. Deconstructing morphology. Acta Zool. 91:44–63.
1048 Schönenberger J., von Balthazar M., López Martínez A., Albert B., Prieu C., Magallón S.,
1049 Sauquet H. 2020. Phylogenetic analysis of fossil flowers using an angiosperm-wide data
1050 set: proof-of-concept and challenges ahead. Am. J. Bot. 107:1433–1448.
1051 Schopf T.J.M. 1984. Rates of evolution and the notion of "living fossils." Annu. Rev. Earth

1052 Planet Sci. 12:245–292.

1053 Seligmann H. 2010. Positive correlations between molecular and morphological rates of

1054 evolution. J Theor Biol. 264:799–807.

1055 Simões T., Vernygora O. V., de Medeiros B.A.S., Wright A.M. 2022a. Handling character

1056 dependency in phylogenetic inference: extensive performance testing of assumptions

1057 and solutions using simulated data. EcoEvoRxiv. DOI: 10.32942/osf.io/r23j8

1058 Simões T.R., Kinney-Broderick G., Pierce S.E. 2022b. An exceptionally preserved

1059 Sphenodon-like sphenodontian reveals deep time conservation of the tuatara skeleton

1060 and ontogeny. Commun. Biol. 5:1–19.

1061 Simões T.R., Vernygora O., Caldwell M.W., Pierce S.E. 2020. Megaevolutionary dynamics

1062 and the timing of evolutionary innovation in reptiles. Nat. Commun. 11:1–14.

1063 Simpson G.G. 1944. Tempo and Mode in Evolution. New York: Columbia University Press.

1064 Simpson G.G. 1953. The Major Features of Evolution. Columbia University Press.

1065 Skilling J. 2006. Nested sampling for general Bayesian computation. Bayesian Anal. 1:833–

1066 860.

1067 Šmarda P., Veselý P., Šmerda J., Bureš P., Knápek O., Chytrá M. 2016. Polyploidy in a

1068 “living fossil” Ginkgo biloba. New Phytol. 212:11–14.

1069 Stanley S.M. 1975. A theory of evolution above the species level. Proc. Natl. Acad. Sci. U. S.

1070 A. 72:646–650.

1071 Subramanian S., Hay J.M., Mohandesan E., Millar C.D., Lambert D.M. 2009. Molecular and

1072 morphological evolution in tuatara are decoupled. Trends Genet. 25:16–18.

1073 Tarasov S. 2019. Integration of anatomy ontologies and evo-devo using structured Markov

1074 models suggests a new framework for modeling discrete phenotypic traits. Syst. Biol.

1075 68:698–716.

1076 Turner D.D. 2019. In defense of living fossils. Biol. Philos. 34:1–22.

1077 Wanninger A. 2015. Morphology is dead - long live morphology! Integrating
1078 MorphoEvoDevo into molecular EvoDevo and phylogenomics. Front. Ecol. Evol. 3:1–9.
1079 Welch J.J., Waxman D. 2008. Calculating independent contrasts for the comparative study of
1080 substitution rates. J. Theor. Biol. 251:667–678.
1081 West-Eberhard M.J. 1989. Phenotypic plasticity and the origins of diversity. Annu. Rev.
1082 Ecol. Syst. Vol. 20.:249–278.
1083 Wright A.M., Hillis D.M. 2014. Bayesian analysis using a simple likelihood model
1084 outperforms parsimony for estimation of phylogeny from discrete morphological data.
1085 PLoS One. 9:e109210.
1086 Zhang Y., Mao F., Mu H., Huang M., Bao Y., Wang L., Wong N.-K., Xiao S., Dai H., Xiang
1087 Z., Ma M., Xiong Y., Zhang Z., Zhang L., Song X., Wang F., Mu X., Li J., Ma H.,
1088 Zhang Y., Zheng H., Simakov O., Yu Z. 2021. The genome of *Nautilus pompilius*
1089 illuminates eye evolution and biomineralization. Nat. Ecol. Evol. 5:927–938.